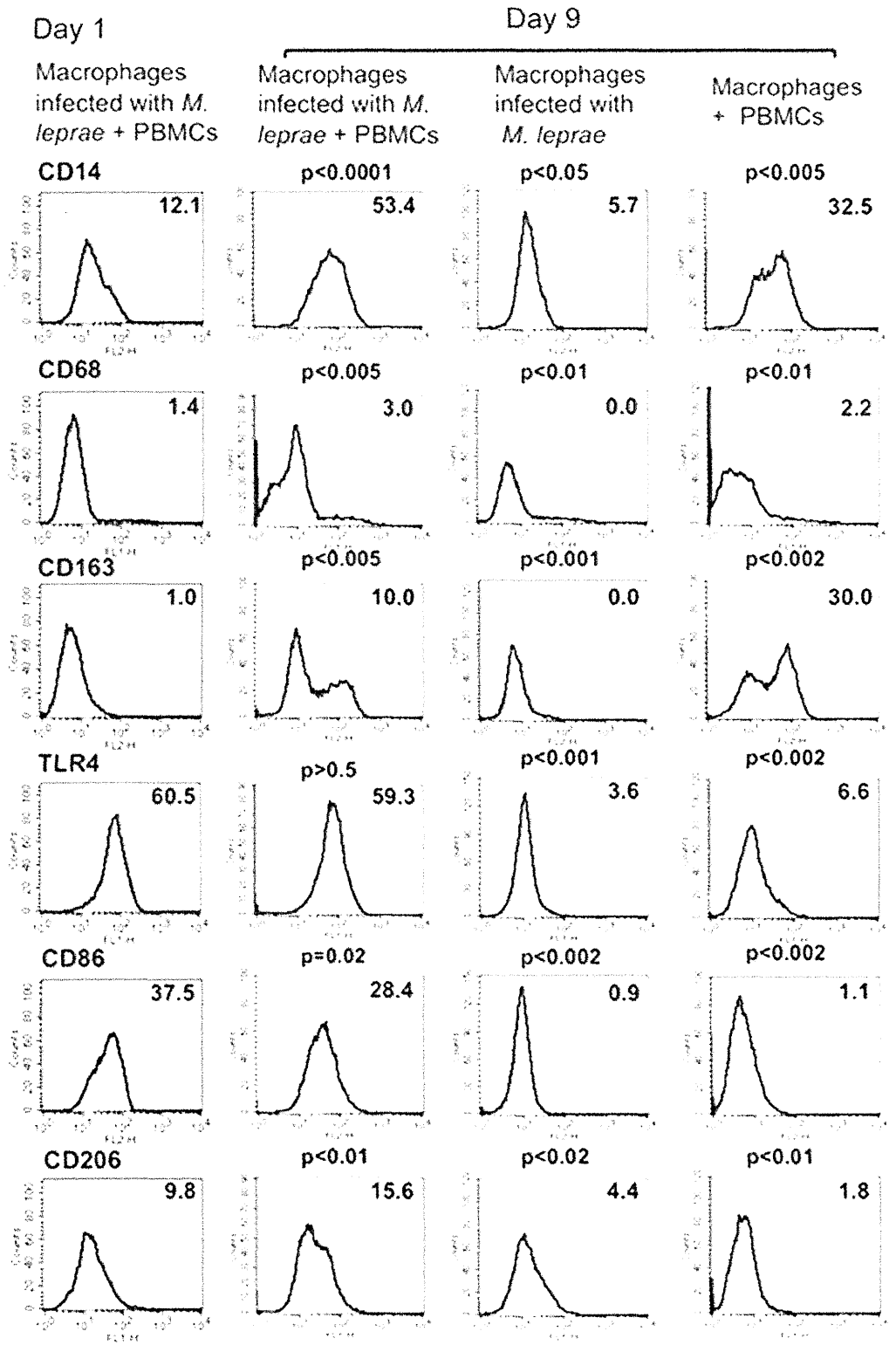

Figure 3 (See legend on next page.)

(See figure on previous page.)
Figure 3 Expression of cell surface antigens on macrophages at two different time points. Compared with the control group on day 1, day 9 macrophages infected with *M. leprae* and co-cultured with T lymphocytes showed relatively higher expression of CD14, CD163 and CD206. While in macrophages infected with *M. leprae*, the expression level of CD14, CD68, CD163, TLR4, CD86 and CD206, were downregulated as compared to those infected macrophages co-cultured with PBMCs. Representative data of one donor, from three independent experiments are shown. P-values were calculated using the Welch unpaired t-test in comparison with day 1 macrophages.

Cytokines in culture supernatants

The culture supernatants from different groups were collected on days 1, 3 and 9 after the start of macrophage culture. The release of IFN-γ, IL-2, TNF-α, IL-12p40, IL-1β, IL-4 and IL-13, was evaluated by ELISA (Figure 4). Interestingly, the expression levels of the various cytokines in supernatants, from different groups showed significant differences that were associated with the formation of granuloma-like aggregates and changes of cell surface antigen expression on macrophages. In the group with *M. leprae* infected macrophages co-cultured with PBMCs, the concentrations of IL-2, IL-1β and TNF-α peaked on day 1 after infection and then declined gradually. The level of IL-12 p40 also declined slowly by day 9. IFN-γ levels were low on day 1, but increased 7 fold by day 4, and then remained unchanged till day 9. A high level of IL-10 expression in macrophages and macrophages cultured with PBMCs was observed, but the expression was significantly decreased when macrophages were infected with *M. leprae* as observed in the day 9 cytokine expression levels. However, when macrophages were differentiated with M-CSF, the expression of IL-10 was significantly high when macrophages were infected with *M. leprae* (Additional file 1: Figure S1). IL-4 and IL-13 were not detected in any groups on days 1 and 9 from the start of macrophage culture (data not shown). Real time PCR results further confirmed the cytokine expression and showed similar results except for the IL-2 and TNF-α, whose expression was observed in control groups of macrophages infected with *M. leprae* in addition to those co-cultured with PBMCs (Figure 5).

The viability of *M. leprae* in granuloma-like aggregates

We determined the viability of *M. leprae* at days 1 and 9, when granuloma-like aggregates were observed in co-cultures of *M. leprae* infected macrophages with PBMCs, whereas in cultures of macrophages infected with *M. leprae*, there was no granuloma formation. The amount of radioactive CO_2 evolved which reflects the rate of ^{14}C-palmitic acid oxidized by *M. leprae*, which was measured by a scintillation counter. No significant difference in $^{14}CO_2$

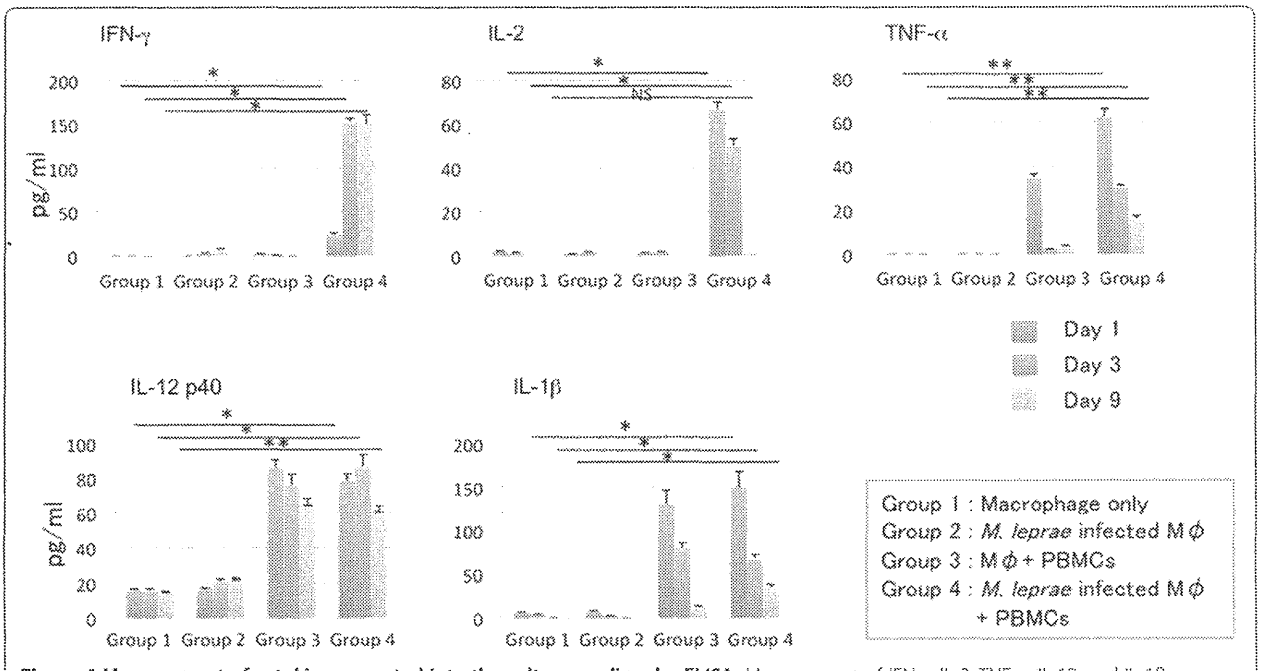

Figure 4 Measurement of cytokines secreted into the culture medium by ELISA. Measurement of IFN-γ, IL-2, TNF-α, IL-12, and IL-1β secreted in the culture medium from different groups of cells at day 1, 3 and 9. Representative data from three individual experiments of a single donor are shown. Unpaired Student's t-test was performed. NS: not significant, *$p < 0.001$, **$p < 0.01$.

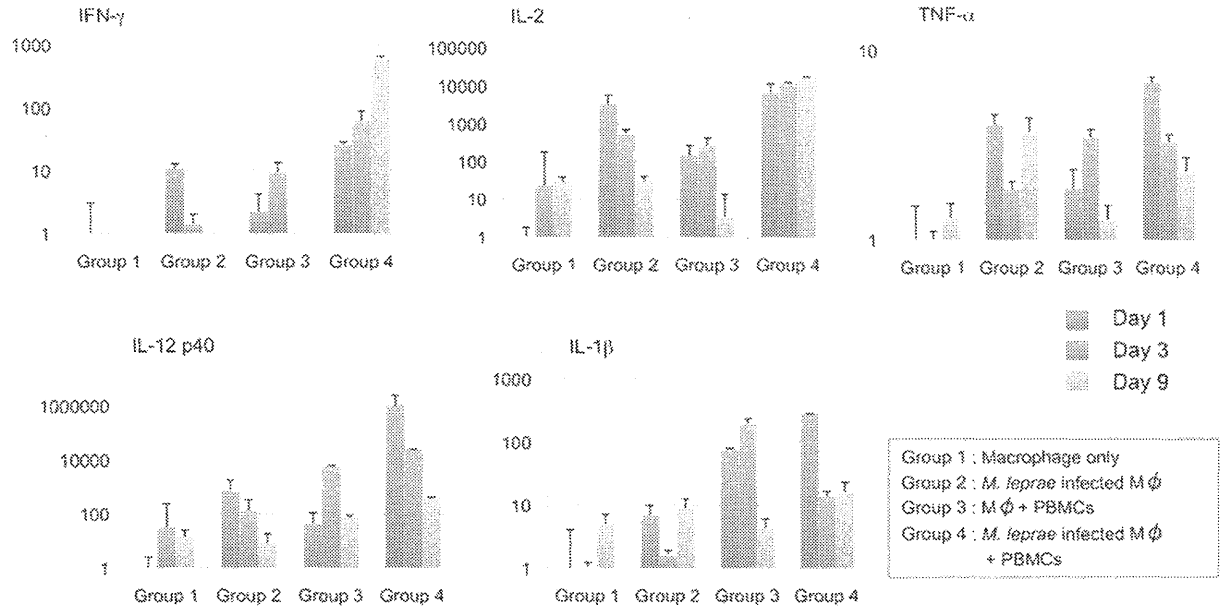

Figure 5 Determination of mRNA level of cytokines by real-time PCR. mRNA expression of IFN-γ, IL-2, TNF-α, IL-12, and IL-1β in the cells was evaluated by using specific primers, SYBR Green PCR Master Mix, and a StepOnePlus (Applied Biosystems). Cells were collected on days 1, 3 and 9 after co-culture with or without PBMCs. The y-axis shows the relative quantitative values calculated from comparative Ct values normalized to the control (actin used as calibrator). The standard deviation of the ΔCt value was determined (Applied Biosystems). Representative data from a single donor of three individual experiments are shown.

production was observed from macrophage in either groups on days 1, and 9. However, the amount of radioactive CO_2 released from macrophages infected with *M. leprae* and co-cultured with PBMCs for 9 days was lower but not significantly lower than that released from macrophages infected with *M. leprae* alone (Figure 6).

Discussion

In the 1960s, Ridley and Jopling proposed a histological classification scheme for leprosy [26]. At one extreme, called the polar tuberculoid, leprosy patients show a high degree of cell-mediated immunity, lesions revealing well-developed granulomatous inflammation and rarely acid-fast bacilli are detected. At the other extreme, termed polar lepromatous patients have no apparent resistance to *M. leprae*, and skin biopsies reveal sheets of foamy macrophages in the dermis containing very large numbers of bacilli and microcolonies called globi. Currently, the formation and maintenance of granulomas are considered to be critical components of the host response to *M. leprae* infection, which determine not only whether primary disease occurs, but also the clinical manifestation. Granuloma formation is studied in mouse models but little is known about the human granuloma due to the ethical problems of using human samples and the difficulties in establishing a good model using human cell lines.

The formation of small, rounded granuloma-like-structure, was previously described by co-culture of blood lymphocytes with autologous macrophages infected with *M. tuberculosis*, or BCG or stimulation with other mycobacterial antigen such as purified protein derivatives. These granuloma-like structures showed abundance of CD68 positive macrophages with small round lymphocytes scattered throughout the

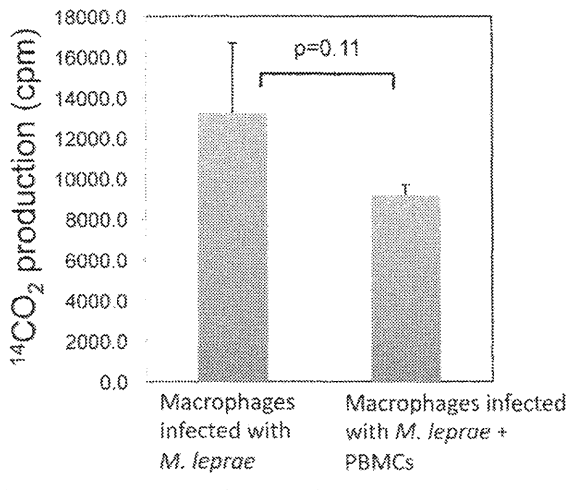

Figure 6 Measurement of the viability of *M. leprae* in macrophages after co-culture with PBMCs. At day 9 after culture of macrophages infected *M. leprae* with or without PBMCs, macrophages were lysed, and the viability of *M. leprae* was determined by a radiorespirometric assay. Unpaired Student's t test was used to determine the statistical significance of the two data sets. Representative data of three individual experiments are shown.

granuloma [15,16]. These models not only exhibit structural similarities to granulomas observed in human clinical specimens, but also show patterns of cell antigen expression and/or cytokine production that appear consistent with those observed in tuberculosis patients. However, the formation of granulomas in leprosy, involving *M. leprae* infection has not been previously studied in vitro. The only data available on granuloma formation of leprosy is from the immunological staining of biopsies of patients, and granulomas harvested from the footpads of athymic nude mice [27].

In our model, we first infected the immature human macrophages with *M. leprae*. To mimic the recruitment of additional PBMCs which would occur in vivo, autologous PBMCs were added after 24 h and cultured at 35° C, the optimal temperature for the growth of *M. leprae* and macrophages to be kept viable. Within 9 days of culture, macrophages and T lymphocytes gathered to form a granuloma-like aggregates with fused macrophages, appearing as multinucleated cells, and epitheloid macrophages tightly linked to surrounding macrophages and lymphocytes. However, in control groups, the formation of granuloma-like aggregates was not observed. When autologous T lymphocytes and monocytes were purified and used instead of PBMCs, a similar formation of granuloma like aggregates were observed, together with production of the same amounts of cytokines, indicating that T lymphocytes and monocytes are sufficient for the containment of *M. leprae* in granuloma like structures.

Electron microscopy studies indicated that the tuberculoid lesion had an appearance of a granulomatous response with a predominance of ECs and MGCs, and the mononuclear phagocytes which are surrounded by a mantle of lymphocytes [28]. In the present *in vitro* model of granulomas, MGCs were prominent, and resembled MGCs observed in a tuberculoid lesion. MGCs have been described by Langhans, but the function of these cells in the granuloma remains to be elucidated [29]. In this study, we observed not only Langhans giant cells (MGCs with a circular nuclear organization in contrast to the MGCs formed in response to a foreign body that lacks this kind of organization), but also the bacilli surrounded by nuclei and restricted to the central cytoplasmic region. Because this type of MGC is not observed in the normal mouse model, it is interesting to further focus on the formation, mechanism and function of such MGCs using human *in vitro* model or humanized mouse model as recently described by Heuts et al. [30]. The *in vitro* model of leprosy granulomas still needs to be investigated, and compared to that obtained using leprosy patients' monocytes and T cells.

Macrophages function as control switches of the immune system, providing a balance between pro- and anti-inflammatory responses by developing into subsets of M1 or M2 activated macrophages. M1 macrophages are activated by type I cytokines such as IFN-γ and TNFα, Alternatively, activated M2 macrophages are subdivided further into M2a (activated by IL-4 or IL-13), M2b (activated by immune complexes in combination with IL-1β) and M2c (activated by IL-10 or glucocorticoids) [31]. M1 macrophages exhibit a potent microbicidal activity, and release IL-12, promoting strong Th1 immune responses. It is the M1 population that is thought to contribute to macrophage-mediated tissue injury [19,32]. In contrast, M2 macrophages support Th2-associated effector functions and exert a selective immunosuppressive activity. M2 macrophages also play a role in the resolution of inflammation through phagocytosis of apoptotic neutrophils, reduced production of pro-inflammatory cytokines, and increased synthesis of mediators that are important for tissue remodeling and wound repair. We investigated the contribution of the macrophage polarization, MGC formation and immune responses against *M. leprae* in granulomas, and found that there was a strong relationship between the formation of granuloma-like aggregates, the changes of cell surface antigen expression on macrophages, and the expression levels of various cytokines with the macrophage polarization. In *M. leprae* infected macrophages co-cultured with PBMCs, the concentrations of IL-2, IL-12 and TNF-α peaked at day 1, while, TLR4, CD86, and MHC molecules were highly expressed, indicating that most of the macrophages were of the M1 subset. At day 9, in the same group of infected macrophages co-cultured with PBMCs, the cells assembled and formed a multilayer, granuloma-like aggregates, and the macrophages not only highly expressed TLR4 and CD86, but also scavenger receptor (CD163) and mannose receptor (CD206) molecules. CD163 and CD206 are the markers of M2 macrophages. Therefore, the M1 and M2 macrophages coexisted in granuloma-like aggregates. Consistent with this observation, the levels of IL-1β, IL-2, IL-12 and IFN-γ were high in the culture medium, promoting the differentiation of macrophages into both M1 and M2 subsets. The protective cell mediated immune response is regulated by the cytokine equilibrium, while the tuberculoid pole is characterized by the presence of Th1 cytokines (IL-2, IFN-γ, TNF-α and IL-12), and lepromatous is characterized by type 2 cytokines (IL-4, IL-6 and IL-10) [33]. Because IL-10 is an immunosuppressive cytokine implicated in susceptibility to mycobacterial infection, we examined the expression of IL-10 in more detail. Indeed, the infection with *M. leprae* suppressed the production of IL-10. However, when macrophages were differentiated with M-CSF, rather than GM-CSF, *M. leprae* infection further enhanced IL-10 production. Our results indicate that the granuloma aggregates studied here, are similar to those observed in the tuberculoid form of leprosy. However, little is known about the type

of cytokines that influence the formation of macrophages for containment of *M. leprae* in the granulomas during the pathogenesis of leprosy.

We also investigated the viability of *M. leprae* in macrophages at different time points. At day 9, a number of granuloma-like aggregates were observed in co-cultures of PBMCs with macrophages infected with *M. leprae.* However in macrophages infected with *M. leprae* without the PBMCs, granuloma-like aggregates were not observed. There were no significant differences in the viability of *M. leprae* in macrophage of different groups on day 1, but on day 9, the viability of *M. leprae* in the group that formed granuloma-like aggregates was slightly lower, although not significantly, than that of *M. leprae* in infected macrophages without PBMCs. Evidently, granuloma-like aggregates appear to benefit the host but the bacilli remained metabolically active. The mechanism of this phenomenon needs further in-depth analysis.

Conclusions

In summary, we have developed for the first time a method to obtain *in vitro M. leprae* granulomas using human monocyte derived macrophages and PBMCs. Using this model, we obtained some basic information about the characteristics of *in vitro* granulomas. In addition, the viability of *M. leprae* in granuloma-like aggregates remained unaltered during the culture period. Effective strategies to allow the bacilli to succumb to the formation of granuloma may assist in the primary control of the infection.

Additional file

Additional file 1: Figure S1. Measurement of IL-10 secreted into the culture medium by ELISA. Measurement of IL-10 secreted in the culture medium from different groups of cells at days 2, 6 and 9 is shown. Two types of macrophages were used to analyze the data. (A) Macrophages differentiated using GM-CSF, and (B) macrophages differentiated from monocytes using M-CSF. Representative data from two individual experiments of a single donor are shown. Unpaired student's t test was performed, *$p < 0.0001$, **$p < 0.001$, ***$p < 0.05$.

Abbreviations

DCs: Dendritic cells; PBMCs: Peripheral blood mononuclear cells; ECs: Epitheloid cells; MGCs: Multinucleated giant cells; BCG: Bacillus Calmette- Guérin.

Competing interests

The authors declare that they have no competing interests.

Authors' contributions

HW, YM participated in the design of the study and carried out the cell culture experiments, YF carried out the confocal microscopic examination, and radio-respirometric assay. HW, YM, and MM were involved in the preparation of the manuscript. All authors have read and approved the final manuscript.

Acknowledgments

This study was supported by grants from the Grant-in-Aid from the Ministry of Health, Labor and Welfare of Japan for "Research on Emerging and Re-emerging Infectious Diseases" (Grant no. H24-Shinko-Ippan-009 to YM) and also from the National Natural Science Foundation of China (30972651), the fund for Key Clinical Program of the Ministry of Health (2010-2012-125). We appreciate the helpful assistance of Drs. Masanori Matsuoka and Masanori Kai for the *M. leprae* propagation and isolation. We also thank the Japanese Red Cross Society for kindly providing whole blood cells from healthy donors.

Author details

[1]Institute of Dermatology, Chinese Academy of Medical Sciences and Peking Union Medical College, 12 Jiangwangmiao Road, Nanjing 210042, China. [2]Department of Mycobacteriology, Leprosy Research Center, National Institute of Infectious Diseases, 4-2-1 Aobacho, Higashimurayama, Tokyo 189-0002, Japan.

Received: 13 December 2012 Accepted: 17 June 2013
Published: 20 June 2013

References

1. Britton WJ: **Immunology of leprosy.** *Trans R Soc Trop Med Hyg* 1993, 87:508–514.
2. Kaplan G, Cohn ZA: **The immunobiology of leprosy.** *Int Rev Exp Pathol* 1986, 28:45–78.
3. Saunders BM, Cooper AM: **Restraining mycobacteria: role of granulomas in mycobacterial infections.** *Immunol Cell Biol* 2000, 78:334–341.
4. Rojas-Espinosa O, Løvik M: ***Mycobacterium leprae* and *Mycobacterium lepraemurium* infections in domestic and wild animals.** *Rev Sci Tech* 2001, 20:219–251.
5. Ulrichs T, Kaufmann SH: **New insights into the function of granulomas in human tuberculosis.** *J Pathol* 2006, 208:261–269.
6. Clay H, Volkman HE, Ramakrishnan L: **Tumor necrosis factor signaling mediates resistance to mycobacteria by inhibiting bacterial growth and macrophage death.** *Immunity* 2008, 29:283–294.
7. Dannenberg AM Jr: **Immunopathogenesis of pulmonary tuberculosis.** *Hosp Pract (Off Ed)* 1993, 28(1):51–58.
8. Lesley R, Ramakrishnan L: **Insights into early mycobacterial pathogenesis from the zebrafish.** *Curr Opin Microbiol* 2008, 11:277–283.
9. Tobin DM, Ramakrishnan L: **Comparative pathogenesis of *Mycobacterium marinum* and *Mycobacterium tuberculosis*.** *Cell Microbiol* 2008, 10:1027–1039.
10. Davis JM, Ramakrishnan L: **The role of the granuloma in expansion and dissemination of early tuberculous infection.** *Cell 2009*, 136:37–49.
11. Bouley DM, Ghori N, Mercer KL, Falkow S, Ramakrishnan L: **Dynamic nature of host-pathogen interactions in *Mycobacterium marinum* granulomas.** *Infect Immun* 2001, 69:7820–7831.
12. Saunders BM, Frank AA, Orme IM, Cooper AM: **CD4 is required for the development of a protective granulomatous response to pulmonary tuberculosis.** *Cell Immunol* 2002, 216:65–72.
13. Poey C, Verhaegen F, Giron J, Lavayssiere J, Fajadet P, Duparc B: **High resolution chest CT in tuberculosis: evolutive patterns and signs of activity.** *J Comput Assist Tomogr* 1997, 21:601–607.
14. Tsai MC, Chakravarty S, Zhu G, Xu J, Tanaka K, Koch C, Tufariello J, Flynn J, Chan J: **Characterization of the tuberculous granuloma in murine and human lungs: cellular composition and relative tissue oxygen tension.** *Cell Microbiol* 2006, 8:218–232.
15. Puissegur MP, Botanch C, Duteyrat JL, Delsol G, Caratero C, Altare F: **An in vitro dual model of mycobacterial granulomas to investigate the molecular interactions between mycobacteria and human host cells.** *Cell Microbiol* 2004, 6:423–433.
16. Birkness KA, Guarner J, Sable SB, Tripp RA, Kellar KL, Bartlett J, Quinn FD: **An in vitro model of the leukocyte interactions associated with granuloma formation in *Mycobacterium tuberculosis* infection.** *Immunol Cell Biol* 2007, 5:160–168.
17. Krausgruber T, Blazek K, Smallie T, Alzabin S, Lockstone H, Sahgal N, Hussell T, Feldmann M, Udalova IA: **IRF5 promotes inflammatory macrophage polarization and TH1-TH17 responses.** *Nat Immunol* 2011, 12:231–238.
18. Satoh T, Takeuchi O, Vandenbon A, Yasuda K, Tanaka Y, Kumagai Y, Miyake T, Matsushita K, Okazaki T, Saitoh T, Honma K, Matsuyama T, Yui K, Tsujimura T, Standley DM, Nakanishi K, Nakai K, Akira S: **The Jmjd3-Irf4 axis regulates M2 macrophage polarization and host responses against helminth infection.** *Nat Immunol* 2010, 11:936–944.

19. Benoit M, Desnues B, Mege JL: **Macrophage polarization in bacterial infections.** *J Immunol* 2008, **181**:3733–3739.
20. Makino M, Baba M: **A cryopreservation method of human peripheral blood mononuclear cells for efficient production of dendritic cells.** *Scand J Immunol* 1997, **45**:618–622.
21. Maeda Y, Mukai T, Spencer J, Makino M: **Identification of an immunomodulating agent from *Mycobacterium leprae*.** *Infect Immun* 2005, **73**:2744–2750.
22. Levy L, Ji B: **The mouse foot-pad technique for cultivation of *Mycobacterium leprae*.** *Lepr Rev* 2006, **77**:5–24.
23. McDermott-Lancaster RD, Ito T, Kohsaka K, Gueipa-Lauras CC, Grosset JH: **Multiplication of *Mycobacterium leprae* in the nude mouse, and some applications of nude mice to experimental leprosy.** *Int J Lepr Other Mycobact Dis* 1987, **55**:889–895.
24. Hashimoto K, Maeda Y, Kimura H, Suzuki K, Masuda A, Matsuoka M, Makino M: ***Mycobacterium leprae* infection in monocyte-derived dendritic cells and its influence on antigen-presenting function.** *Infect Immun* 2002, **70**:5167–5176.
25. Truman RW, Krahenbuhl JL: **Viable *Mycobacterium leprae* as a research reagent.** *Int J Lepr Other Mycobact Dis* 2001, **69**:1–12.
26. Ridley DS, Jopling WH: **Classification of leprosy according to immunity. A five-group system.** *Int J Lepr Other Mycobact Dis* 1966, **34**:255–273
27. Hagge DA, Ray NA, Krahenbuhl JL, Adams LB: **An in vitro model for the lepromatous leprosy granuloma: Fate of *Mycobacterium leprae* from target macrophages after interaction with normal and activated effector macrophages.** *J Immunol* 2004, **172**:7771–7779.
28. Kaplan G, Van Voorhis WC, Sarno EN, Nogueira N, Cohn ZA: **The cutaneous infiltrates of leprosy. A transmission electron microscopy study.** *J Exp Med* 1983, **158**:1145–1159.
29. Postlethwaite AE, Jackson BK, Beachey EH, Kang AH: **Formation of multinucleated giant cells from human monocyte precursors. Mediation by a soluble protein from antigen-and mitogen-stimulated lymphocytes.** *J Exp Med* 1982, **155**:168–178.
30. Heuts F, Gavier-Widen D, Carow B, Juarez J, Wigzell H, Rottenberg ME: **CD4+ cell dependent granuloma formation in humanized mice infected with mycobacteria.** *PNAS* 2013, **110**:6482–6487.
31. Laskin DL: **Macrophages and Inflammatory Mediators in Chemical Toxicity: A Battle of Forces.** *Chem Res Toxicol* 2009, **22**:1376–1385.
32. Trujillo G, O'Connor EC, Kunkel SL, Hogaboam CM: **A novel mechanism for CCR4 in the regulation of macrophage activation in bleomycin-induced pulmonary fibrosis.** *Am J Pathol* 2008, **172**:1209–1221.
33. Yamamura M, Wang XH, Ohmen JD, Uyemura K, Rea TH, Bloom BR, Modlin RL: **Cytokine patterns of immunologically mediated tissue damage.** *J Immunol* 1992, **149**:1470–1475.

doi:10.1186/1471-2334-13-279
Cite this article as: Wang *et al.*: **An *in vitro* model of *Mycobacterium leprae* induced granuloma formation.** *BMC Infectious Diseases* 2013 **13**:279.

nature immunology

Phosphorylation of the adaptor ASC acts as a molecular switch that controls the formation of speck-like aggregates and inflammasome activity

Hideki Hara[1,5], Kohsuke Tsuchiya[1,5], Ikuo Kawamura[1], Rendong Fang[1], Eduardo Hernandez-Cuellar[1], Yanna Shen[1,2], Junichiro Mizuguchi[3], Edina Schweighoffer[4], Victor Tybulewicz[4] & Masao Mitsuyama[1]

The inflammasome adaptor ASC contributes to innate immunity through the activation of caspase-1. Here we found that signaling pathways dependent on the kinases Syk and Jnk were required for the activation of caspase-1 via the ASC-dependent inflammasomes NLRP3 and AIM2. Inhibition of Syk or Jnk abolished the formation of ASC specks without affecting the interaction of ASC with NLRP3. ASC was phosphorylated during inflammasome activation in a Syk- and Jnk-dependent manner, which suggested that Syk and Jnk are upstream of ASC phosphorylation. Moreover, phosphorylation of Tyr144 in mouse ASC was critical for speck formation and caspase-1 activation. Our results suggest that phosphorylation of ASC controls inflammasome activity through the formation of ASC specks.

Inflammasomes are large multiprotein oligomers that serve critical roles in host defense against microbial pathogens and the development of inflammatory disorders by facilitating the secretion of proinflammatory cytokines[1]. Core components of each inflammasome are pro-caspase-1 and a cytosolic pattern-recognition receptor belonging to the Nod-like receptor (NLR) family or the HIN-200 family, which contains a pyrin domain or a caspase-recruitment domain (CARD). Inflammasome complexes are believed to be assembled after the recognition of specific stimuli by the receptors[2,3]. Once assembled, inflammasomes serve as platforms for the activation of caspase-1, which in turn cleaves the precursor forms of interleukin-1β (IL-1β) and IL-18 to their bioactive forms[4].

Different subsets of inflammasomes are activated by different stimuli. The NLRC4 inflammasome is activated by flagellin and the type III secretion apparatus from bacteria[5–7]. Anthrax lethal toxin produced by *Bacillus anthracis* triggers activation of the NLRP1B inflammasome in mouse macrophages[8]. Activation of the NLRP3 inflammasome depends on a priming step (signal 1) and an activation step (signal 2)[9]. Signal 1 can be induced by signaling via Toll-like receptors, whereas signal 2 is induced by microbial components with diverse molecular structures, such as microbial RNA and toxins[10,11]. In addition, the adjuvant alum and endogenous danger-associated molecules, including ATP and monosodium urate (MSU) crystals, also induce signal 2 for the activation of the NLRP3 inflammasome[10,12,13]. AIM2 and IFI16 sense cytosolic DNA and nuclear DNA, respectively, and DNA viruses[14], *Francisella tularensis*[15], *Listeria monocytogenes*[16,17] and *Streptococcus pneumoniae*[18] have been demonstrated to activate the AIM2 inflammasome or IFI16 inflammasome[19] in host cells.

The adaptor ASC (PYCARD or TMS-1) is composed of a pyrin domain and a CARD and contributes to the assembly of inflammasome complexes[20]. ASC serves as the bridge between pro-caspase-1 and pyrin-containing inflammasomes, such as NLRP3 and AIM2. Accordingly, NLRP3 and AIM2 require ASC exclusively for the recruitment of pro-caspase-1, while the CARD-containing receptors NLRC4 and NLRP1 can directly interact with pro-caspase-1 (refs. 1,7,21). During inflammasome activation, ASC also forms cytosolic macromolecular aggregates of ASC dimers called 'ASC specks', 'ASC foci' or 'pyroptosomes'[22,23]. The ASC speck recruits and activates pro-caspase-1, which leads to the secretion of large amounts of IL-1β and IL-18 and to pyroptosis, a form of programmed cell death. However, ASC is not always essential for cytokine processing and the induction of pyroptosis via the NLRC4 inflammasome. In addition to protein-protein interactions in inflammasome complexes, published reports have revealed the involvement of type I interferons[15,24], the ubiquitin ligase–associated protein SGT1, the heat-shock protein hsp90 (ref. 25), unidentified serine proteases[26] and kinases[27–33], such as PKC-δ, PKR, Syk, Lyn, PI(3)K, Erk and DAPK, in the activation or regulation of inflammasomes, but how these molecules participate in inflammasome activity remains largely unclear.

Given the importance of the protective and pathological roles of inflammasomes, it is worth clarifying what and how signaling factors are involved in the activation of inflammasomes. Here we found that the NLRP3 and AIM2 inflammasomes, but not the NLRC4 inflammasome, required Syk and Jnk for their full activity. Inhibition of Syk or Jnk abolished the NLRP3- or AIM2-mediated formation of ASC specks without affecting the interaction between ASC and NLRP3.

[1]Department of Microbiology, Kyoto University Graduate School of Medicine, Kyoto, Japan. [2]School of Laboratory Medicine, Tianjin Medical University, Tianjin, China. [3]Department of Immunology and Intractable Immunology Research Center, Tokyo Medical University, Tokyo, Japan. [4]MRC National Institute for Medical Research, London, UK. [5]H.H. and K.T. contributed equally to this work. Correspondence should be addressed to M.M. (mituyama@mb.med.kyoto-u.ac.jp).

Received 10 April; accepted 27 September; published online 3 November 2013; doi:10.1038/ni.2749

We also found that ASC underwent Syk- and Jnk-dependent phosphorylation and that Tyr144, one of the possible phosphorylation sites, was critical for speck formation. Our results indicate the phosphorylation of ASC may be an additional target for controlling inflammasome activity.

RESULTS

NLRP3 and AIM2 require Syk and Jnk for IL-18 secretion

To examine the role of kinases in inflammasome activation, we assessed the effects of a series of common kinase inhibitors (**Supplementary Table 1**) on the NLRP3, AIM2 and NLRC4 inflammasomes in peritoneal macrophages. To rule out the possibility of effects of the inhibitors on signal 1 delivered by priming with lipopolysaccharide (LPS), we added the inhibitors to macrophage cultures 3 h after the initiation of LPS priming. Those inhibitors did not affect the abundance of the inflammasome components or of pro-IL-18 or pro-IL-1β at the protein level (**Supplementary Fig. 1a**). We measured IL-18 secretion as an indicator of caspase-1 activation, as pro-IL-18, unlike pro-IL-1β, is constitutively expressed in macrophages[31]. The nigericin-induced secretion of IL-18 from macrophages was significantly lower after pretreatment with an inhibitor of Syk or Jnk, but not after pretreatment with inhibitors of other kinases, than after pretreatment with dimethyl sulfoxide, as a control (**Fig. 1a**). We obtained similar results with mouse bone marrow–derived macrophages and the U937 human macrophage cell line (**Supplementary Fig. 1b,c**), which excluded the possibility of macrophage type– and species-specific effects. The production of IL-18 induced by alum, another NLRP3 activator, was also diminished by pretreatment with an inhibitor of Syk or Jnk (**Supplementary Fig. 1e**), which suggested that Syk and Jnk contributed to activation of the NLRP3 inflammasome. Moreover, we found that the production of IL-18 induced by the synthetic B-form double-stranded DNA poly(dA:dT), but not that induced by flagellin, was substantially inhibited by pretreatment with an inhibitor of Syk or Jnk (**Fig. 1b,c**). To confirm the role of Syk and Jnk in this, we used small interfering RNA to knock down the expression of *Syk* or the genes encoding Jnk1 and Jnk2 (*Mapk8-Mapk9*) in macrophages, and also assessed macrophages with knockout of *Syk*, *Mapk8* or *Mapk9*, and found that either knockdown or knockout decreased the secretion of IL-18 in response to nigericin or poly(dA:dT) (**Fig. 1d–h** and **Supplementary Fig. 2a–d**). Also, the nigericin-induced secretion of IL-1β from macrophages was reduced by an inhibitor of Syk or Jnk or knockout of either *Syk* or *Mapk8-Mapk9* (**Fig. 1e** and **Supplementary Fig. 1d**). Those observations suggested involvement of Syk and Jnk in activation of the NLRP3 and AIM2 inflammasomes. Syk deficiency in macrophages resulted in a moderate decrease in the secretion of IL-18 and IL-1β induced by nigericin (**Fig. 1d,e**), which indicated that Syk was not a critical requirement for activation of the NLRP3 inflammasome but instead contributed to that. *Salmonella enterica* serovar Typhimurium 14028 (*S.* Typhimurium) and *Mycobacterium tuberculosis* strain H37Rv are recognized mainly by NLRC4 and NLRP3, respectively, while *Listeria monocytogenes* strain EGD is recognized by various receptors, including AIM2 and NLRP3 (refs. 6,17,33). Consistent with the results reported above obtained by stimulation by ligands, IL-18 production induced by *S.* Typhimurium was not affected much by inhibition of Syk or Jnk in macrophages, whereas IL-18 production induced by *M. tuberculosis* or *L. monocytogenes* was reduced by inhibition of Syk or Jnk (**Fig. 1i–k**). From these

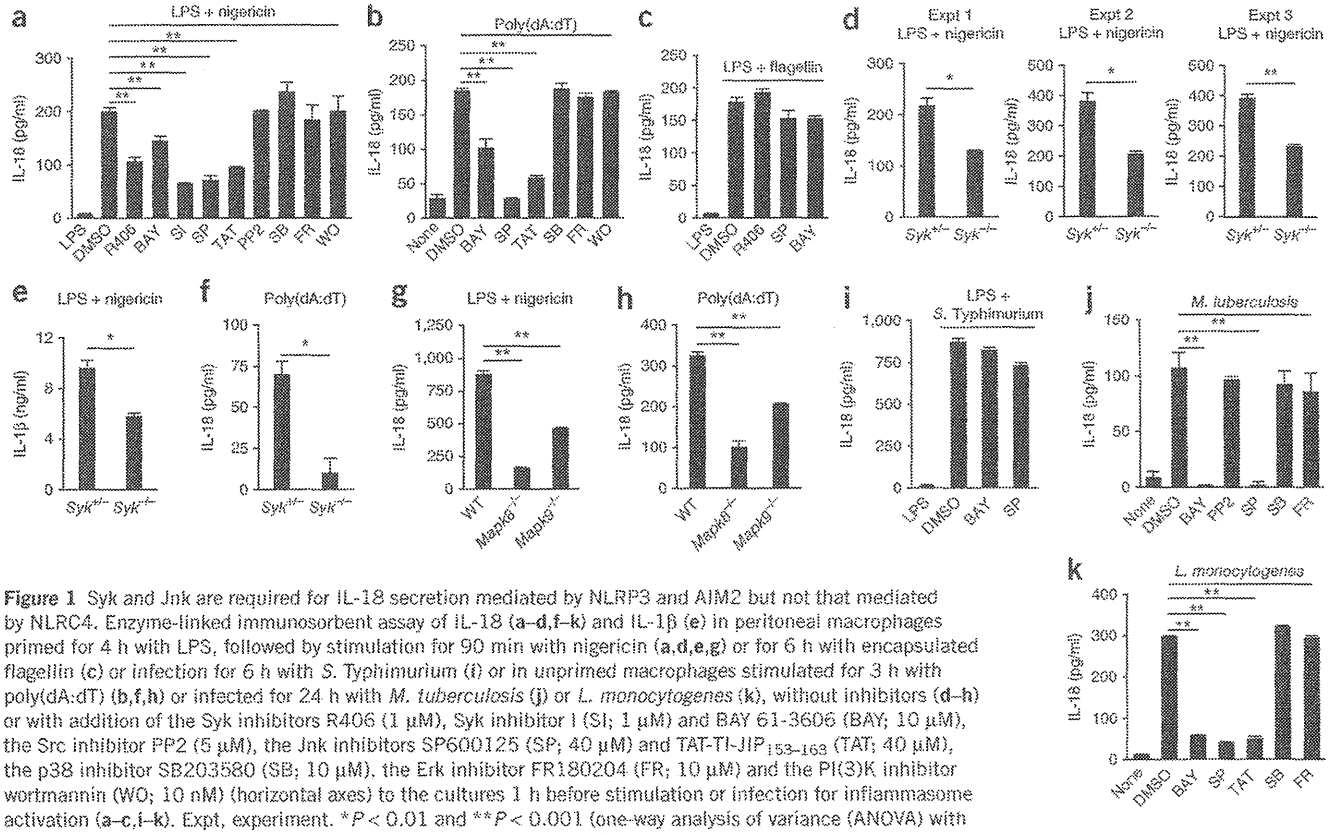

Figure 1 Syk and Jnk are required for IL-18 secretion mediated by NLRP3 and AIM2 but not that mediated by NLRC4. Enzyme-linked immunosorbent assay of IL-18 (**a–d,f–k**) and IL-1β (**e**) in peritoneal macrophages primed for 4 h with LPS, followed by stimulation for 90 min with nigericin (**a,d,e,g**) or for 6 h with encapsulated flagellin (**c**) or infection for 6 h with *S.* Typhimurium (**i**) or in unprimed macrophages stimulated for 3 h with poly(dA:dT) (**b,f,h**) or infected for 24 h with *M. tuberculosis* (**j**) or *L. monocytogenes* (**k**), without inhibitors (**d–h**) or with addition of the Syk inhibitors R406 (1 μM), Syk inhibitor I (SI; 1 μM) and BAY 61-3606 (BAY; 10 μM), the Src inhibitor PP2 (5 μM), the Jnk inhibitors SP600125 (SP; 40 μM) and TAT-TI-JIP$_{153–163}$ (TAT; 40 μM), the p38 inhibitor SB203580 (SB; 10 μM), the Erk inhibitor FR180204 (FR; 10 μM) and the PI(3)K inhibitor wortmannin (WO; 10 nM) (horizontal axes) to the cultures 1 h before stimulation or infection for inflammasome activation (**a–c,i–k**). Expt, experiment. $^*P < 0.01$ and $^{**}P < 0.001$ (one-way analysis of variance (ANOVA) with Bonferroni's multiple-comparison test (**a–c,g–k**) or two-tailed unpaired *t*-test with Welch's correction (**d–f**)). Data are representative of at least three independent experiments (**a–f,i–k**) or two independent experiments (**g,h**; mean and s.d. of triplicates).

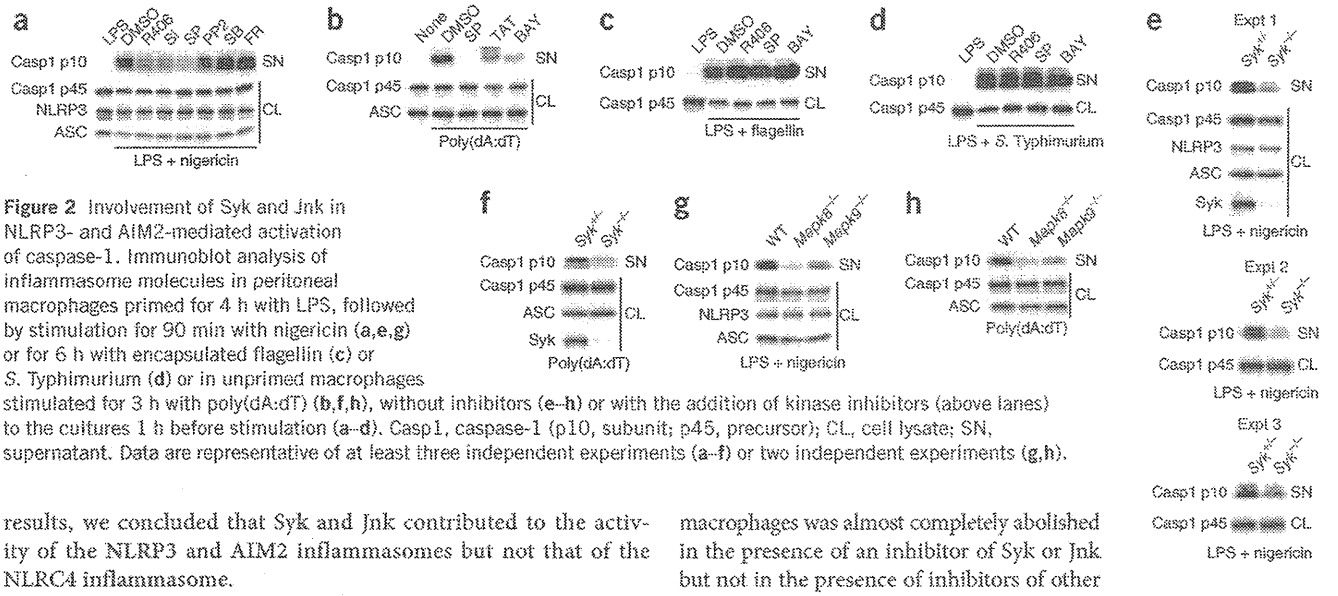

Figure 2 Involvement of Syk and Jnk in NLRP3- and AIM2-mediated activation of caspase-1. Immunoblot analysis of inflammasome molecules in peritoneal macrophages primed for 4 h with LPS, followed by stimulation for 90 min with nigericin (**a**,**e**,**g**) or for 6 h with encapsulated flagellin (**c**) or *S.* Typhimurium (**d**) or in unprimed macrophages stimulated for 3 h with poly(dA:dT) (**b**,**f**,**h**), without inhibitors (**e**–**h**) or with the addition of kinase inhibitors (above lanes) to the cultures 1 h before stimulation (**a**–**d**). Casp1, caspase-1 (p10, subunit; p45, precursor); CL, cell lysate; SN, supernatant. Data are representative of at least three independent experiments (**a**–**f**) or two independent experiments (**g**,**h**).

results, we concluded that Syk and Jnk contributed to the activity of the NLRP3 and AIM2 inflammasomes but not that of the NLRC4 inflammasome.

Caspase-1 activation requires Syk and Jnk

Next we assessed the involvement of Syk and Jnk in the activation of caspase-1 via the NLRP3 and AIM2 inflammasomes. Activation of caspase-1 induced by nigericin, alum or poly(dA:dT) in peritoneal macrophages was almost completely abolished in the presence of an inhibitor of Syk or Jnk but not in the presence of inhibitors of other kinases (**Fig. 2a,b** and **Supplementary Fig. 1f**). In contrast, we did not observe effects of those two inhibitors on the activation of caspase-1 induced by flagellin or *S.* Typhimurium (**Fig. 2c,d**). Furthermore, activation of caspase-1 induced by nigericin or poly(dA:dT) was reduced in Syk- or Jnk-deficient macrophages and by knockdown of those kinases

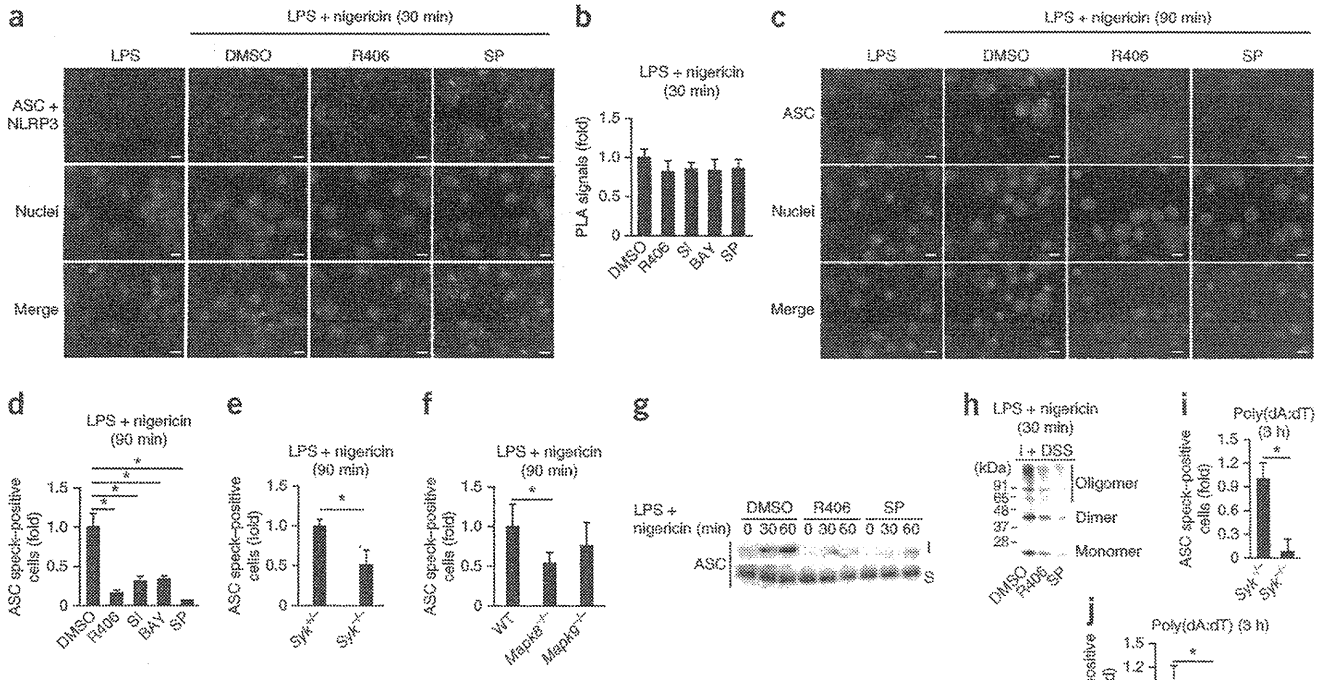

Figure 3 Requirement for signaling via Syk and Jnk for ASC aggregation. (**a**–**h**) *In situ* PLA of ASC-NLRP3 complexes (**a**,**b**), ASC staining (**c**–**f**) and immunoblot analysis of ASC (**g**,**h**) in peritoneal macrophages primed for 4 h with LPS, followed by stimulation for various times (above) with nigericin in the presence or absence of kinase inhibitors. (**a**,**c**) ASC-NLRP3 complexes, red (**a**); ASC, green (**c**); nuclei, blue (**a**,**c**). Scale bars, 10 μm. (**b**) Quantification of PLA signals per cell, presented relative to that of control cells treated with solvent. (**d**–**f**) Quantification of cells with ASC specks, presented relative to that of control cells treated with solvent or wild-type cells. (**g**,**h**) Triton-soluble (S) and Triton-insoluble (I) fractions (right margin; **g**) or Triton-insoluble fractions treated with disuccinimidyl suberate (I + DSS; **h**). (**i**,**j**) ASC staining in unprimed macrophages stimulated for 3 h with poly(dA:dT), presented as in **d**–**f**. *$P < 0.001$ (Kruskal-Wallis test with Dunn's multiple-comparison test (**b**,**j**), one-way ANOVA with Bonferroni's multiple-comparison test (**d**,**f**), two-tailed unpaired *t*-test with Welch's correction (**e**) or Mann-Whitney test (**i**)). Data are representative of at least three independent experiments (**a**–**d**,**g**,**h**) or two independent experiments (**e**,**f**,**i**,**j**; mean and s.d. of triplicates in **b**,**d**–**f**,**i**,**j**).

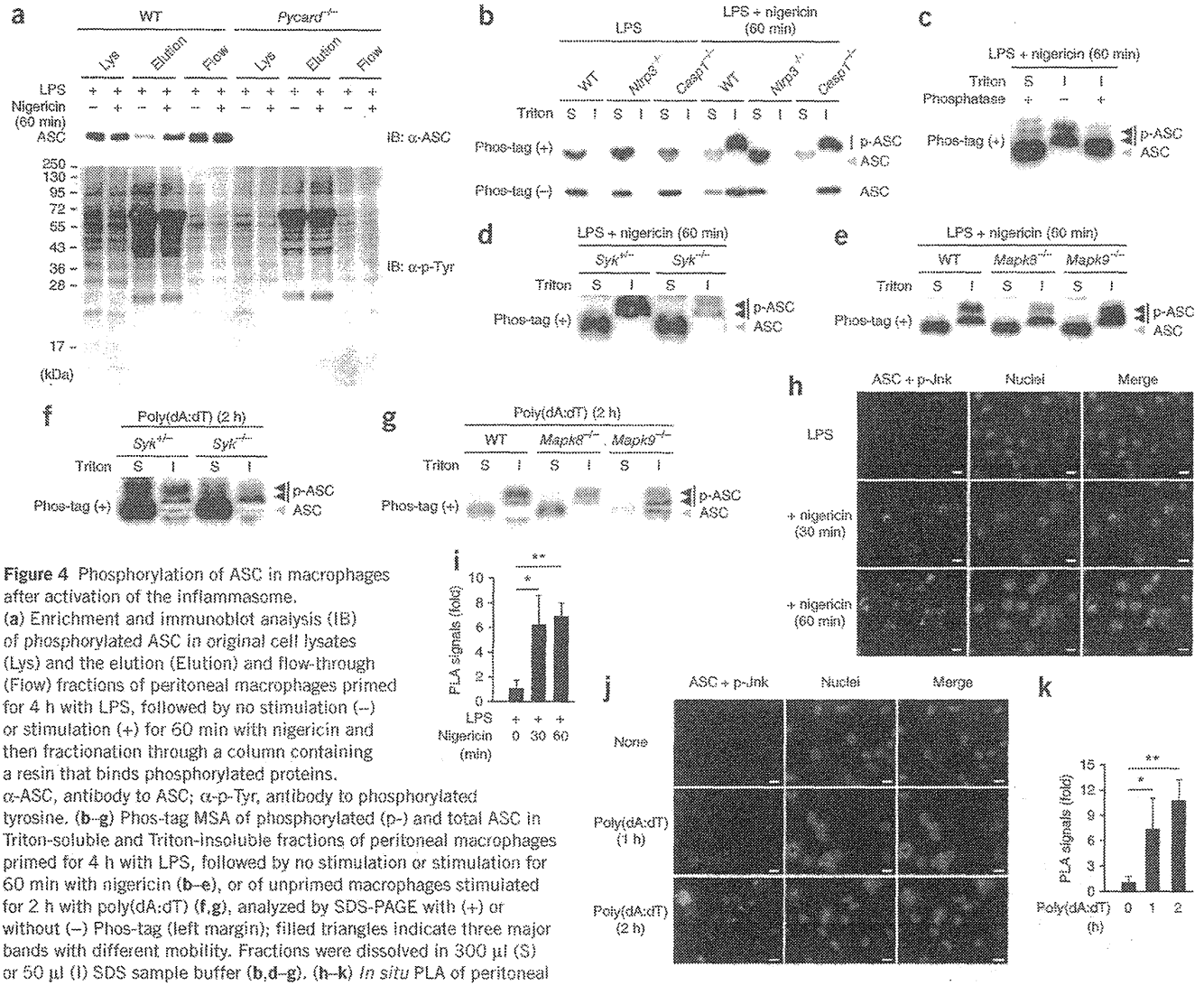

Figure 4 Phosphorylation of ASC in macrophages after activation of the inflammasome. (**a**) Enrichment and immunoblot analysis (IB) of phosphorylated ASC in original cell lysates (Lys) and the elution (Elution) and flow-through (Flow) fractions of peritoneal macrophages primed for 4 h with LPS, followed by no stimulation (–) or stimulation (+) for 60 min with nigericin and then fractionation through a column containing a resin that binds phosphorylated proteins. α-ASC, antibody to ASC; α-p-Tyr, antibody to phosphorylated tyrosine. (**b**–**g**) Phos-tag MSA of phosphorylated (p-) and total ASC in Triton-soluble and Triton-insoluble fractions of peritoneal macrophages primed for 4 h with LPS, followed by no stimulation or stimulation for 60 min with nigericin (**b**–**e**), or of unprimed macrophages stimulated for 2 h with poly(dA:dT) (**f**,**g**), analyzed by SDS-PAGE with (+) or without (–) Phos-tag (left margin); filled triangles indicate three major bands with different mobility. Fractions were dissolved in 300 μl (S) or 50 μl (I) SDS sample buffer (**b**,**d**–**g**). (**h**–**k**) *In situ* PLA of peritoneal macrophages primed for 4 h with LPS, followed by stimulation for 0–60 min with nigericin (**h**,**i**) or of unprimed macrophages stimulated for 0–2 h with poly(dA:dT) (**j**,**k**). (**h**,**j**) Red, complexes of ASC with phosphorylated Jnk (ASC + p-Jnk); blue, nuclei. Scale bars, 10 μm. (**i**,**k**) Results presented relative to those of unstimulated control cells. $^{*}P < 0.01$ and $^{**}P < 0.001$ (Kruskal-Wallis test with Dunn's multiple-comparison test (**i**) or one-way ANOVA with Tukey-Kramer multiple-comparison test (**k**)). Data are representative of two (**a**,**c**,**e**–**g**) or three (**b**,**d**,**h**–**k**) independent experiments (mean and s.d. of triplicates in **i**,**k**).

mediated by small interfering RNA (**Fig. 2e–h** and **Supplementary Fig. 2e,f**). The activation of caspase-1 induced by *M. tuberculosis* or *L. monocytogenes* in macrophages was lower after treatment with an inhibitor Syk or Jnk than after treatment with the dimethyl sulfoxide control (data not shown). These results suggested that Syk and Jnk signals were involved in the activation of caspase-1 through the NLRP3 and AIM2 inflammasomes but not in the NLRC4 inflammasome–dependent activation of caspase-1.

Syk is not required for NLRP3 inflammasome in dendritic cells

It has been reported that Syk is not required for nigericin-induced activation of the NLRP3 inflammasome in dendritic cells[28]. Consistent with that report, we observed no significant difference between wild-type and Syk-deficient bone marrow–derived dendritic cells in caspase-1 activation or IL-18 secretion in response to nigericin (**Supplementary Fig. 3a,c,d**). In contrast, IL-18 secretion and caspase-1 activation induced by nigericin were lower in Syk-deficient peritoneal macrophages and bone marrow–derived macrophages than in $Syk^{+/+}$ or $Syk^{+/-}$ cells (**Figs. 1d,e** and **2e** and **Supplementary Fig. 3b,e**). This suggested that the requirement for Syk in NLRP3 activation in response to nigericin was cell type specific.

Syk and Jnk regulate inflammasomes via unknown pathways

We investigated whether inflammasome-activating agents induced activation of Syk and Jnk, assessed by the detection of phosphorylated kinases. Stimulation with nigericin or poly(dA:dT) induced detectable levels of phosphorylated Syk and Jnk (**Supplementary Fig. 4a–d**). The phosphorylation of Jnk induced by nigericin or poly(dA:dT) was not reduced by inhibitors of Syk or in Syk-deficient peritoneal macrophages (**Supplementary Fig. 4e–g**), which suggested that Syk is not upstream of Jnk in this process. Syk is reported to serve a pivotal role in activation of the NLRP3 inflammasome in response to *Candida albicans* by inducing the generation of reactive oxygen species (ROS) and CARD9-dependent activation of the transcription factor NF-κB[28]. However, we

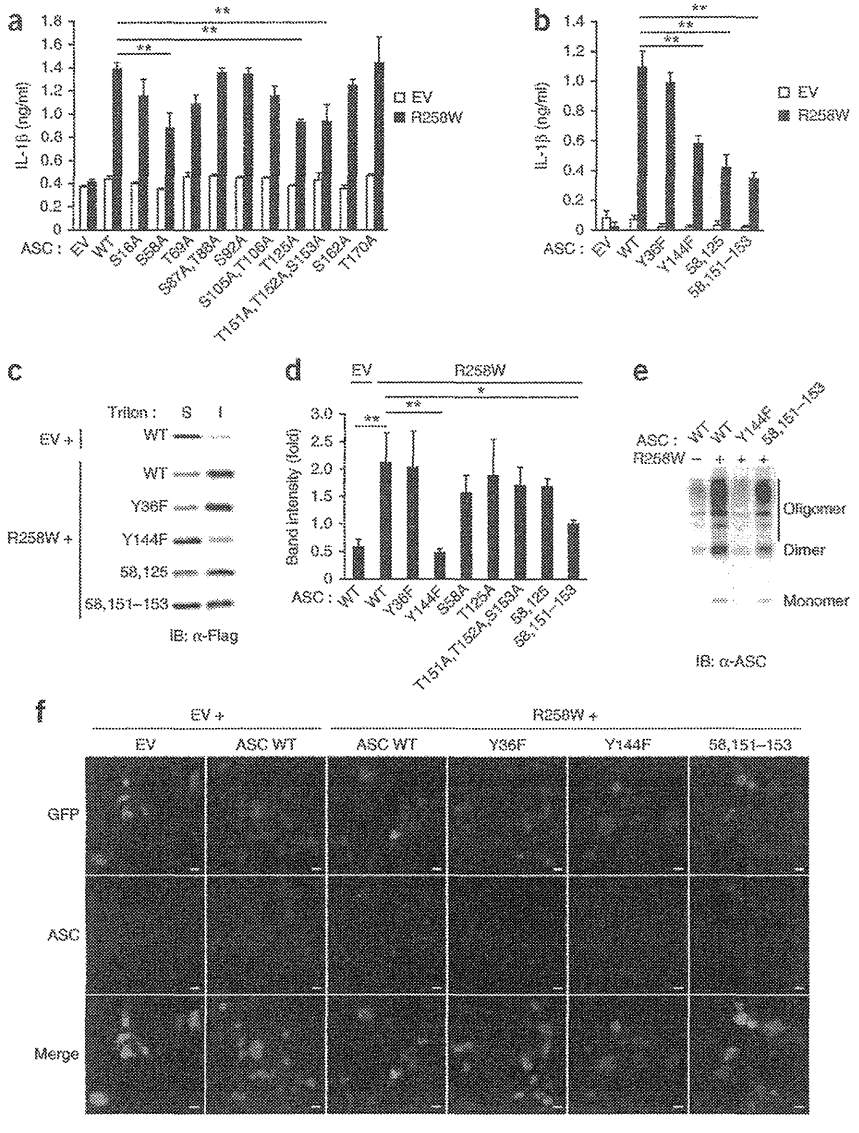

Figure 5 Identification of amino acid residues in ASC critical for its biological activities. (**a**,**b**) Enzyme-linked immunosorbent assay of IL-1β in HEK293 cells 48 h after reconstitution by transfection of empty vector (EV) or vector encoding Flag-tagged NLRP3(R258W) (100 ng) (key) along with empty vector or vector encoding Flag-tagged wild-type (WT) or mutant ASC (10 ng; horizontal axes), plus vector encoding pro-caspase-1 (30 ng) and pro-IL-1β (100 ng). 58,125, ASC(S58A) with the additional substitution T125A. (**c**–**e**) Immunoblot analysis (**c**,**e**) and quantification (**d**) of ASC in Triton-soluble and Triton-insoluble fractions (**c**,**d**) and disuccinimidyl suberate–treated Triton-insoluble fractions (**e**) of reconstituted HEK293 cells 48 h after transfection of empty vector or vector encoding Flag-tagged NLRP3(R258W) (left margin (**c**), top (**d**) or above lanes (**e**)) along with vector encoding Flag-tagged wild-type or mutant ASC (left margin (**c**), horizontal axis (**d**) or above lanes (**e**)); in **d**, band intensity of insoluble ASC is presented relative to that of soluble ASC. (**f**) ASC staining in HEK293 cells treated as in **c**–**e**: red, ASC; green, transfected cells (visualized by transfection of a plasmid encoding green fluorescent protein (100 ng)). Scale bars, 10 μm. $^*P < 0.05$ and $^{**}P < 0.001$ (one-way ANOVA with Bonferroni's multiple-comparison test (**a**,**b**) or Tukey-Kramer's multiple-comparison test (**d**)). Data are from one experiment representative of three independent experiments (mean and s.d. of triplicates in **a**,**b**,**d**).

observed that wild-type and CARD9-deficient macrophages produced similar levels of IL-18 in response to nigericin or poly(dA:dT) and that the ROS scavenger BHA did not affect activation of the AIM2 inflammasome in macrophages (**Supplementary Fig. 4h–j**). Moreover, the expression of mitochondrial ROS, which is important for the activation of NLRP3, was not reduced by an inhibitor of Syk or Jnk in nigericin-stimulated macrophages (**Supplementary Fig. 4k**). These results indicated that Syk- and Jnk-dependent activation of the inflammasome is not mediated by ROS or CARD9 and that Syk and Jnk operate in a different pathway(s).

The formation of ASC specks requires Syk and Jnk

Both NLRP3 and AIM2 require the common adaptor ASC to recruit and activate pro-caspase-1 (ref. 1). We therefore speculated that Syk and Jnk might be involved in the interaction of ASC with NLRP3 or AIM2. To investigate that possibility, we visualized ASC-NLRP3 complexes by an *in situ* proximity ligation assay (PLA). As reported before[30], we observed small spots of ASC-NLRP3 complexes in peritoneal macrophages, and these increased in abundance after stimulation with nigericin (**Fig. 3a**). The abundance of spots was not increased by stimulation with nigericin in the absence of ASC or NLRP3 (data not shown), which suggested that ASC-NLRP3 complexes were specifically visualized by this technique. After stimulation with nigericin, the number of spots representing ASC-NLRP3 complexes was similar in macrophages pretreated with an inhibitor of Syk or Jnk and those pretreated with dimethyl sulfoxide (**Fig. 3a**,**b**), which indicated that inhibition of Syk or Jnk did not affect the interaction between NLRP3 and ASC, a critical step in formation of the NLRP3 inflammasome, in macrophages stimulated with nigericin. Next we visualized the formation of ASC specks and found that pretreatment with an inhibitor of Syk or Jnk or deficiency in either Syk or Jnk reduced the nigericin-induced formation of ASC specks in macrophages (**Fig. 3c–f** and **Supplementary Fig. 5a**,**b**). Because ASC has been reported to form Triton X-100–resistant aggregates[20], we prepared Triton X-100–soluble and Triton X-100–insoluble fractions from macrophages to analyze the distribution of ASC. ASC was almost undetectable in the Triton X-100–insoluble fraction of LPS-primed macrophages but was significantly greater in abundance after stimulation with nigericin (**Fig. 3g**). Moreover, most ASC in the Triton X-100–insoluble fraction was a dimer or oligomer[15] (**Fig. 3h**). Pretreatment with an inhibitor of Syk or Jnk reduced the redistribution of ASC induced by nigericin and also resulted in a decrease in the amount of dimerized and oligomerized ASC (**Fig. 3g**,**h**). We obtained similar results for macrophages stimulated with poly(dA:dT) (**Fig. 3i**,**j** and **Supplementary Fig. 5c–f**). These results suggested that signaling by Syk and Jnk was required for the formation of ASC specks but not for the NLR-ASC interaction.

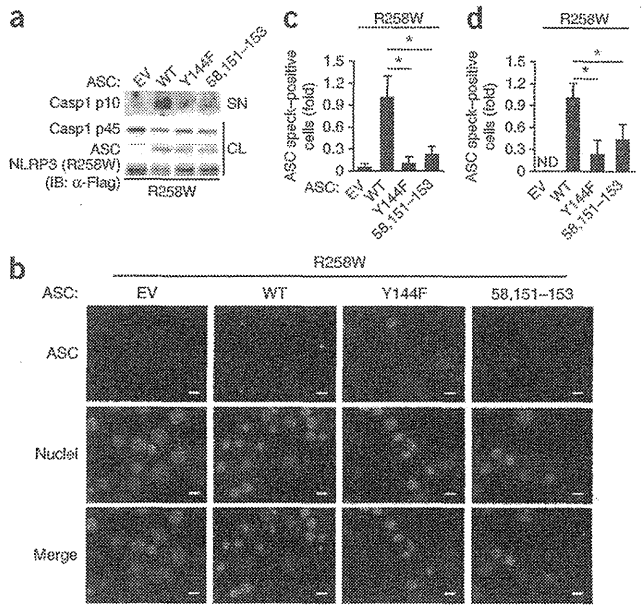

Figure 6 Critical roles of the possible phosphorylation sites of ASC in macrophages. (**a**–**c**) Immunoblot analysis of inflammasome molecules (**a**), ASC staining (**b**) and quantification of ASC specks (**c**) in reconstituted RAW264.7 cells 9 h after transfection of vector encoding Flag-tagged NLRP3(R258W) plus empty vector or vector encoding wild-type or mutant ASC (above lanes or images (**a**,**b**) or horizontal axis (**c**)). (**b**) ASC, green; nuclei, blue. Scale bars, 10 μm. (**c**) Results presented relative to those of the cells transfected with empty vector. (**d**) Quantification of ASC specks in primary *Pycard*$^{-/-}$ peritoneal macrophages 9 h after reconstitution by transfection of vector encoding Flag-tagged NLRP3(R258W) plus empty vector or vector encoding Flag-tagged ASC (presented as in **c**). ND, not detected. *$P < 0.001$ (one-way ANOVA with Bonferroni's multiple-comparison test (**c**,**d**)). Data are from one experiment representative of three independent experiments (mean and s.d. of triplicates in **c**,**d**).

Phosphorylation of ASC after inflammasome activation

A published report has implied that ASC undergoes phosphorylation in response to inflammatory stimuli[34]. To investigate whether the aggregate formation of ASC was regulated by its phosphorylation mediated by Syk and Jnk during inflammasome activation, we enriched phosphorylated proteins from macrophage lysates through the use of a column containing a phosphorylated protein–binding resin and then detected ASC by immunoblot analysis. We observed that stimulation with nigericin induced an increase in the amount of ASC in the elution fraction (with enrichment for phosphorylated proteins; **Fig. 4a**). To further analyze the phosphorylation of ASC, we obtained Triton X-100–soluble and Triton X-100–insoluble cell lysates and analyzed them by a mobility-shift assay (MSA) based on the phosphate-binding tag Phos-tag[35]. In these gels, ASC in the Triton X-100–insoluble fraction migrated more slowly than that in the Triton X-100–soluble fraction, and the shift in mobility was reversed by phosphatase treatment (**Fig. 4b**,**c**), which suggested that ASC in the former fraction was phosphorylated. We observed the slowly migrating ASC in the Triton X-100–insoluble fraction of caspase-1-deficient macrophages but not in that of NLRP3-deficient macrophages, after stimulation with nigericin (**Fig. 4b**), which suggested that the increase in phosphorylated ASC in response to nigericin required NLRP3 but not caspase-1. ASC may be phosphorylated at multiple sites, as we detected three major bands with different mobility (**Fig. 4c**–**g**).

In addition, deficiency in either Syk or Jnk decreased the intensity of the ASC band with the lowest mobility in the Triton X-100–insoluble fraction of macrophages stimulated with nigericin or poly(dA:dT) (**Fig. 4d**–**g**). We obtained similar results with an inhibitor of Syk or Jnk (data not shown). These data suggested that ASC was phosphorylated after activation of the NLRP3 and AIM2 inflammasomes via the Syk and Jnk pathways. Syk and DAPK have been shown to associate with the NLRP3 inflammasome complex[29,30]. Accordingly, we analyzed the interaction of ASC with phosphorylated Jnk by *in situ* PLA. We observed complexes of ASC with phosphorylated Jnk in wild-type macrophages (**Fig. 4h**–**k**), but not in ASC-deficient macrophages (negative control; data not shown), after stimulation with nigericin or poly(dA:dT). Notably, most of the complexes were located in or around the nucleus at later time points (**Fig. 4h**,**j**). These data suggested that ASC was phosphorylated after activation of the NLRP3 and AIM2 inflammasomes via the Syk and Jnk pathways.

Phosphorylation of ASC is critical for inflammasome activation

We next sought to identify ASC-phosphorylation sites that regulate the aggregate formation that results in activation of caspase-1. We detected 14 or 8 possible phosphorylation sites, respectively, in mouse ASC with NetPhos (a neural network–based method for predicting potential phosphorylation sites at serine, threonine or tyrosine residues; version 2.0), at a threshold of 0.5, or with GPS (a group-based prediction system for the computational prediction of phosphorylation sites with their cognate kinases; version 2.1.1) with the low threshold (**Supplementary Fig. 6** and **Supplementary Table 2**). We constructed a series of expression vectors encoding ASC

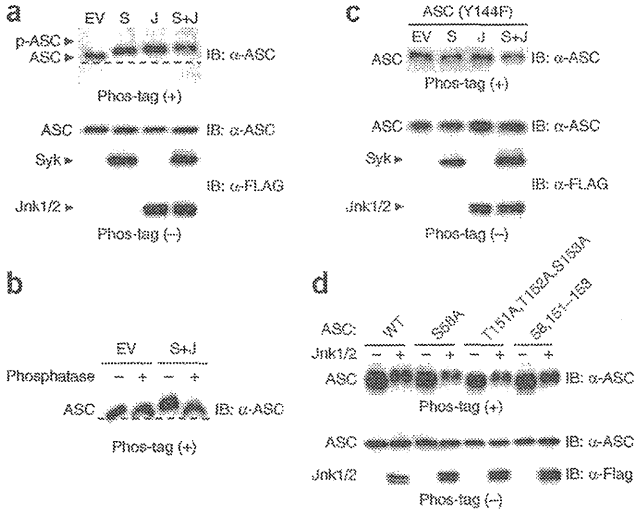

Figure 7 Identification of phosphorylation sites in ASC. (**a**) Phos-tag MSA of reconstituted HEK293 cells 48 h after transfection of vector encoding Flag-tagged wild-type ASC (50 ng) plus empty vector or vector encoding Syk (300 ng) (S) or Jnk1 (300 ng) and Jnk2 (300 ng) (J) or vectors encoding Syk, Jnk1 and Jnk2 (S+J). (**b**) Phos-tag MSA of reconstituted HEK293 cells 48 h after transfection of vector encoding Flag-tagged wild-type ASC plus empty vector or vectors encoding Syk, Jnk1 and Jnk2, followed by no treatment (–) or treatment with phosphatase (+). (**c**) Phos-tag MSA of reconstituted HEK293 cells 48 h after transfection of vector encoding Flag-tagged ASC(Y144F) plus vectors as in **a** (above lanes). (**d**) Phos-tag MSA of reconstituted HEK293 cells 48 h after transfection of vector encoding Flag-tagged wild-type or mutant ASC (top) plus empty vector (–) or vector Jnk1 (300 ng) and Jnk2 (300 ng) (+). Data are representative of three independent experiments.

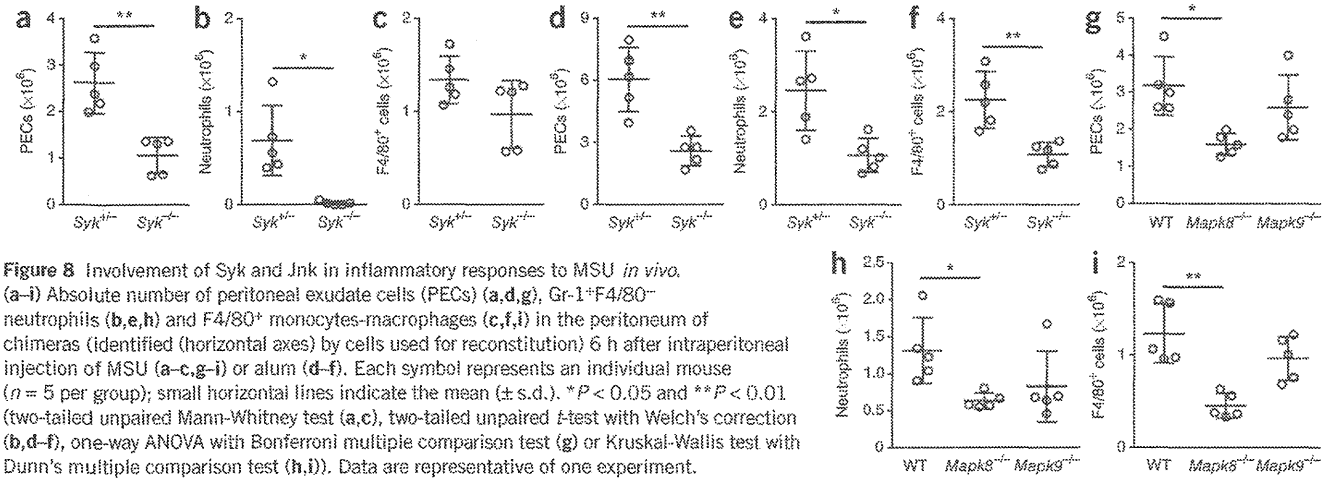

Figure 8 Involvement of Syk and Jnk in inflammatory responses to MSU *in vivo*. (**a–i**) Absolute number of peritoneal exudate cells (PECs) (**a**,**d**,**g**), Gr-1$^+$F4/80$^-$ neutrophils (**b**,**e**,**h**) and F4/80$^+$ monocytes-macrophages (**c**,**f**,**i**) in the peritoneum of chimeras (identified (horizontal axes) by cells used for reconstitution) 6 h after intraperitoneal injection of MSU (**a–c**,**g–i**) or alum (**d–f**). Each symbol represents an individual mouse ($n = 5$ per group); small horizontal lines indicate the mean (± s.d.). $^*P < 0.05$ and $^{**}P < 0.01$ (two-tailed unpaired Mann-Whitney test (**a**,**c**), two-tailed unpaired *t*-test with Welch's correction (**b**,**d–f**), one-way ANOVA with Bonferroni multiple comparison test (**g**) or Kruskal-Wallis test with Dunn's multiple comparison test (**h**,**i**)). Data are representative of one experiment.

mutants in which amino acid residues predicted to be phosphorylated were replaced with alanine or phenylalanine, then assessed the ability of those ASC point mutants to induce IL-1β secretion in an inflammasome-reconstitution system based on HEK293 human embryonic kidney cells (**Supplementary Fig. 7a,b**). We observed that the ability of the point mutants ASC(S58A), ASC(T125A), ASC(Y144F) or ASC(T151A,T152A,S153A) to induce IL-1β secretion in response to NLRP3(R258W), a disease-associated mutant of NLRP3, was slightly lower that of wild-type ASC (**Fig. 5a,b**). We further altered the ASC(S58A) mutant by the additional substitution T125A or with the three additional substitutions of T151A, T152A and S153A (ASC(58,151–153)) and found that IL-1β-inducing ability of the resulting ASC mutants was significantly lower than that of ASC(S58A) (**Fig. 5b**). Furthermore, ASC(Y144F) and ASC(58,151–153) showed less redistribution into the Triton X-100–insoluble fraction in response to NLRP3(R258W) than did wild-type ASC (**Fig. 5c,d**). ASC(Y1-44F) and ASC(58,151–153) were still able to form dimers and oligomers in the Triton X-100–insoluble fraction (**Fig. 5e**), probably because those substitutions affected the redistribution of ASC without affecting its dimerization or oligomerization. Moreover, we found that ASC(Y144F) expressed together with NLRP3(R258W) formed almost no aggregates, in contrast to wild-type ASC expressed together with NLRP3(R258W) (**Fig. 5f**). These results suggested that Tyr144, Ser58, Thr151, Thr152 and Ser153, all putative phosphorylation sites of ASC, were involved in both IL-1β-inducing ability and aggregate formation.

We investigated whether those results obtained with HEK293 cell could be reproduced in the mouse macrophage cell line RAW264.7, which lacks ASC expression. Wild-type ASC expressed together with NLRP3(R258W) in RAW264.7 cells formed speck-like structures and induced the activation of caspase-1, whereas speck formation was diminished in RAW264.7 cells transfected to express ASC(Y144F) or ASC(58,151–153) (**Fig. 6a–c**). The formation of ASC specks was also abrogated by the substitutions in similar experiments with ASC-deficient primary macrophages (**Fig. 6d**).

We further investigated whether those residues were phosphorylated in a Syk- and Jnk-dependent manner. ASC expressed together with either Syk or Jnk migrated more slowly in Phos-tag gels than did ASC in cells transfected with empty vector (**Fig. 7a**). Transfection of cells to express ASC with both Syk and Jnk resulted in a greater mobility shift, which was reversed by phosphatase treatment (**Fig. 7a,b**). These results suggested that ASC was phosphorylated at multiple sites in a Syk- and Jnk-dependent manner. The observed changes in the mobility of ASC in the presence of Syk or Jnk were all abrogated by the Y144F substitution in ASC (**Fig. 7c**). In contrast, the mobility of ASC(S58A), ASC(T151A,T152A,S153A) and ASC(58,151–153) in Phos-tag gels, like that of wild-type ASC, was reduced by overexpression of Jnk1-Jnk2 (**Fig. 7d**), which suggested that Ser58, Thr151, Thr152 and Ser153 were not phosphorylated in a Jnk-dependent manner or that the effect of those substitutions on the mobility may have been masked by phosphorylation at other residues. These results showed that phosphorylation of Tyr144 was required for inflammasome activation.

We did *in vitro* kinase assays with synthetic peptides (amino acids 139–150 of mouse ASC or amino acids 141–152 of human ASC) to investigate the possibility that Syk directly phosphorylates Tyr144 of mouse ASC and the corresponding tyrosine residue of human ASC. We incubated those peptides with ATP in the presence or absence of recombinant Syk and assessed the kinase reaction by the consumption of ATP. We did not observe substantially less ATP in reactions in which we used those ASC peptides as a substrate for recombinant Syk, whereas reactions containing purified tubulin, as a positive control substrate, had less ATP (data not show). Thus, our data did not support or were not sufficient to justify the possibility of direct phosphorylation of Tyr144 by Syk.

MSU- and alum-induced peritonitis is dependent on Syk and Jnk

Next we investigated whether Syk and Jnk were required for inflammasome activation *in vivo*. We analyzed the recruitment of inflammatory cells into the peritoneal cavity as an indicator of stimulant-induced inflammation after intraperitoneal injection of mice with MSU or alum. As shown before[12,29], both MSU and alum strongly induced the recruitment of cells, including Gr-1$^+$ F4/80$^-$ neutrophils and F4/80$^+$ monocytes and macrophages, in an ASC-dependent manner (**Supplementary Fig. 8a–f**). We then reconstituted irradiated wild-type mice with fetal liver cells to generate *Syk*$^{+/-}$ and *Syk*$^{-/-}$ chimeras or with bone marrow cells to generate wild-type, *Mapk8*$^{-/-}$ and *Mapk9*$^{-/-}$ chimeras. After challenge with MSU or alum, *Syk*$^{-/-}$ chimeras had fewer total cells, neutrophils, and monocytes-macrophages in the peritoneal cavity than did *Syk*$^{+/-}$ chimeras (**Fig. 8a,b,d–f**). After challenge with MSU, the number of peritoneal monocytes-macrophages tended to be lower in *Syk*$^{-/-}$ chimeras than in *Syk*$^{+/-}$ chimeras, but the difference between the groups was not statistically significant (**Fig. 8c**). The infiltration of inflammatory cells induced by MSU or alum was also lower in *Mapk8*$^{-/-}$ chimeras or in wild-type mice treated with

an inhibitor of Jnk than in wild-type chimeras or wild-type mice treated with vehicle only, respectively (**Fig. 8g–i** and **Supplementary Fig. 8a–f**). In contrast, the inflammasome-independent infiltration of inflammatory cells induced by chemokine CXCL1 (KC) was similar in $Syk^{+/-}$ and $Syk^{-/-}$ chimeras and in $Mapk8^{+/+}$ and $Mapk8^{-/-}$ chimeras (**Supplementary Fig. 8g–i**), and the inhibitor of Jnk did not reduce the infiltration of inflammatory cells induced by alum in ASC-deficient mice ($n = 3$; data not shown). These results suggested that signaling via Syk and Jnk was involved in the MSU- and alum-induced infiltration of inflammatory cells that was largely dependent on ASC.

DISCUSSION

The phosphorylation and dephosphorylation of proteins is important in controlling a wide range of biological processes, including innate and adaptive immunity and apoptosis[36,37]. The involvement of kinases such as PKC-δ, PKR, Syk, Lyn, PI(3)K, Erk and DAPK in inflammasome activation has been reported, yet the precise mechanism of their action has remained unclear. In particular, Syk has been demonstrated to contribute to the NLRP3 inflammasome in response to *C. albicans*, most probably due to its role in inducing ROS production[28,29,31,33]. NLRC4 is phosphorylated after stimulation with its ligands, and that phosphorylation is critical for inflammasome activation[27]. Here we showed that Syk and Jnk were involved in the activity of ASC-containing inflammasomes in macrophages via a mechanism that regulated the formation of ASC specks. We found that ASC was phosphorylated in a Syk- and Jnk-dependent manner at multiple sites, which most probably included Tyr144, which was essential for speck formation. The phosphorylation of ASC during inflammasome activation was required for activity of the NLRP3 and AIM2 inflammasomes. Thus, inflammasomes are regulated by protein kinases and perhaps by phosphatase(s) that target phosphorylated inflammasome components.

We identified Tyr144 of ASC as a critical residue for speck formation and a possible phosphorylation site. Consistent with that, phosphorylation of the corresponding residue in human ASC (Tyr146) has been disclosed in a patent application (Hornbeck, P. *et al.*, US patent application 2009/0325189 A1). The Y144F substitution in ASC completely abrogated the phosphorylation of ASC induced by overexpression of Syk or Jnk, which suggested that Tyr144 serves as a regulator of ASC phosphorylation mediated by those kinases. That tyrosine residue is evolutionary conserved. Tyr144 is located in the CARD, whereas published studies have shown that the pyrin domain of ASC is phosphorylated after stimulation with tumor-necrosis factor[34], which suggests the existence of other phosphorylation sites that might also contribute to inflammasome activity.

It remains unclear how signaling via Syk and Jnk regulates the formation of ASC specks. Transfection of HEK293 cells to express ASC together with Syk or Jnk or both did not result in the formation of ASC specks or the redistribution of ASC to the Triton X-100–insoluble fraction (data not shown), which suggested that phosphorylation of ASC itself was not sufficient to induce speck formation in the absence of stimuli of the inflammasome. Our results also suggested a crucial role for Syk and Jnk in the redistribution, rather than the dimerization or oligomerization, of ASC upon inflammasome activation. During the generation of ASC aggregates, monomeric ASC, which is diffusely distributed before stimulation, is rapidly translocated to a perinuclear speck in each cell. The formation of ASC specks is prevented by treatment with nocodazole, and ASC specks are located near the microtubule-organizing center[38], which suggests a possible role for microtubules in the migration of ASC during the step of speck formation. In our assays, most complexes of ASC and phosphorylated Jnk were located in or around the nucleus, and ASC remained diffusely distributed in the cytosol even after inflammasome activation in cells in which Syk or Jnk was inhibited genetically or pharmacologically. Thus, we speculate that Syk- and Jnk-mediated ASC phosphorylation may function as a molecular 'switch' that controls the migration of ASC along microtubules to the site of speck formation. Together, these results indicate that ASC speck formation is a consequence of multiple cellular events orchestrated by inflammasome receptors, Syk, Jnk and perhaps microtubules.

Although inflammasomes have pivotal roles in innate immunity to pathogens, excessive or dysregulated activation of inflammasomes, especially the NLRP3 inflammasome, has been linked to various autoinflammatory diseases and autoimmune diseases, including Muckle-Wells syndrome, inflammatory bowel diseases[39,40], vitiligo[41] and rheumatoid arthritis[12]. Inflammasomes have also been linked to obesity-induced insulin resistance[42], atherosclerosis[43] and gouty arthritis[44] and could represent potential targets for therapy. Therapies involving antibody to IL-1β appear to be effective in treating inflammatory disorders associated with deregulated inflammasome activity, and further understanding of the basic processes and mechanisms involved in inflammasome activation will provide additional strategies for controlling autoinflammatory conditions. Here we have shown that phosphorylation of the inflammasome component ASC regulates inflammasome activity. Thus, for example, compounds designated to specifically inhibit the phosphorylation of ASC may be promising drug candidates for the treatment of inflammasome-associated diseases, and antibodies specific to phosphorylated ASC may be useful for diagnostic and research purposes. Further investigation of the inflammasome will reveal the precise roles of kinases in inflammasome activation and may identify additional mechanisms for controlling inflammasome activity.

METHODS

Methods and any associated references are available in the online version of the paper.

Note: Any Supplementary Information and Source Data files are available in the online version of the paper.

ACKNOWLEDGMENTS

We thank J. Tschopp and the Institute for Arthritis Research for permission to use *Nlrp3*$^{-/-}$ mice; S.Taniguchi (Shinshu University) for *Pycard*$^{-/-}$ mice; K. Kuida (Millennium Pharmaceuticals) for *Casp1*$^{-/-}$ mice; T. Saito (RIKEN RCAI) for *Card9*$^{-/-}$ mice; K. Kawasaki (Doshisha Women's College) for *S.* Typhimurium 14028; H. Tsutsui (Hyogo Medical University) for *Nlrp3*$^{-/-}$, *Pycard*$^{-/-}$ and *Casp1*$^{-/-}$ mice; H. Hara (Saga University) for *Card9*$^{-/-}$ mice; M. Matsuura (Kyoto University) for *S.* Typhimurium 14028 and for U937 cells; H. Tanizaki (Kyoto University) for RAW264.7 cells; and K. Sada and Y. Tohyama for advice on Syk experiments. Supported by the Ministry of Education, Culture, Sports, Science and Technology of Japan, the Ministry of Health, Labour and Welfare of Japan, the Japan Society for the Promotion of Science and Medical Research Council UK (U117527252 for E.S. and V.T.).

AUTHOR CONTRIBUTIONS

H.H. initiated the study and designed and did the experiments with macrophages and peritonitis; K.T. designed and did the experiments with HEK293 cells; K.T., H.H. and M.M. wrote the manuscript; I.K. provided advice; R.F., E.H.-C. and Y.S. contributed to the experiments; J.M. provided the *Mapk8*$^{-/-}$ and *Mapk9*$^{-/-}$ mice; E.S. and V.T. provided the *Syk*$^{+/+}$, *Syk*$^{+/-}$ and *Syk*$^{-/-}$ fetal liver cells; and M.M. supervised the project.

COMPETING FINANCIAL INTERESTS

The authors declare no competing financial interests.

1. Martinon, F., Mayor, A. & Tschopp, J. The inflammasomes: guardians of the body. *Annu. Rev. Immunol.* **27**, 229–265 (2009).
2. Brodsky, I.E. & Monack, D. NLR-mediated control of inflammasome assembly in the host response against bacterial pathogens. *Semin. Immunol.* **21**, 199–207 (2009).
3. Davis, B.K., Wen, H. & Ting, J.P. The inflammasome NLRs in immunity, inflammation, and associated diseases. *Annu. Rev. Immunol.* **29**, 707–735 (2011).
4. Dinarello, C.A. Immunological and inflammatory functions of the interleukin-1 family. *Annu. Rev. Immunol.* **27**, 519–550 (2009).
5. Miao, E.A. *et al.* Innate immune detection of the type III secretion apparatus through the NLRC4 inflammasome. *Proc. Natl. Acad. Sci. USA* **107**, 3076–3080 (2010).
6. Franchi, L. *et al.* Cytosolic flagellin requires Ipaf for activation of caspase-1 and interleukin 1β in salmonella-infected macrophages. *Nat. Immunol.* **7**, 576–582 (2006).
7. Miao, E.A. *et al.* Cytoplasmic flagellin activates caspase-1 and secretion of interleukin 1beta via Ipaf. *Nat. Immunol.* **7**, 569–575 (2006).
8. Boyden, E.D. & Dietrich, W.F. Nalp1b controls mouse macrophage susceptibility to anthrax lethal toxin. *Nat. Genet.* **38**, 240–244 (2006).
9. Franchi, L., Munoz-Planillo, R., Reimer, T., Eigenbrod, T. & Nunez, G. Inflammasomes as microbial sensors. *Eur. J. Immunol.* **40**, 611–615 (2010).
10. Mariathasan, S. *et al.* Cryopyrin activates the inflammasome in response to toxins and ATP. *Nature* **440**, 228–232 (2006).
11. Kanneganti, T.D. *et al.* Critical role for Cryopyrin/Nalp3 in activation of caspase-1 in response to viral infection and double-stranded RNA. *J. Biol. Chem.* **281**, 36560–36568 (2006).
12. Martinon, F., Petrilli, V., Mayor, A., Tardivel, A. & Tschopp, J. Gout-associated uric acid crystals activate the NALP3 inflammasome. *Nature* **440**, 237–241 (2006).
13. Li, H., Nookala, S. & Re, F. Aluminum hydroxide adjuvants activate caspase-1 and induce IL-1beta and IL-18 release. *J. Immunol.* **178**, 5271–5276 (2007).
14. Rathinam, V.A. *et al.* The AIM2 inflammasome is essential for host defense against cytosolic bacteria and DNA viruses. *Nat. Immunol.* **11**, 395–402 (2010).
15. Fernandes-Alnemri, T. *et al.* The AIM2 inflammasome is critical for innate immunity to *Francisella tularensis*. *Nat. Immunol.* **11**, 385–393 (2010).
16. Tsuchiya, K. *et al.* Involvement of absent in melanoma 2 in inflammasome activation in macrophages infected with *Listeria monocytogenes*. *J. Immunol.* **185**, 1186–1195 (2010).
17. Kim, S. *et al. Listeria monocytogenes* is sensed by the NLRP3 and AIM2 inflammasome. *Eur. J. Immunol.* **40**, 1545–1551 (2010).
18. Fang, R. *et al.* Critical roles of ASC inflammasomes in caspase-1 activation and host innate resistance to *Streptococcus pneumoniae* infection. *J. Immunol.* **187**, 4890–4899 (2011).
19. Kerur, N. *et al.* IFI16 acts as a nuclear pathogen sensor to induce the inflammasome in response to Kaposi sarcoma-associated herpesvirus infection. *Cell Host Microbe* **9**, 363–375 (2011).
20. Masumoto, J. *et al.* ASC, a novel 22-kDa protein, aggregates during apoptosis of human promyelocytic leukemia HL-60 cells. *J. Biol. Chem.* **274**, 33835–33838 (1999).
21. Case, C.L., Shin, S. & Roy, C.R. Asc and Ipaf Inflammasomes direct distinct pathways for caspase-1 activation in response to *Legionella pneumophila*. *Infect. Immun.* **77**, 1981–1991 (2009).
22. Bryan, N.B., Dorfleutner, A., Rojanasakul, Y. & Stehlik, C. Activation of inflammasomes requires intracellular redistribution of the apoptotic speck-like protein containing a caspase recruitment domain. *J. Immunol.* **182**, 3173–3182 (2009).
23. Fernandes-Alnemri, T. *et al.* The pyroptosome: a supramolecular assembly of ASC dimers mediating inflammatory cell death via caspase-1 activation. *Cell Death Differ.* **14**, 1590–1604 (2007).
24. Guarda, G. *et al.* Type I interferon inhibits interleukin-1 production and inflammasome activation. *Immunity* **34**, 213–223 (2011).
25. Mayor, A., Martinon, F., De Smedt, T., Petrilli, V. & Tschopp, J. A crucial function of SGT1 and HSP90 in inflammasome activity links mammalian and plant innate immune responses. *Nat. Immunol.* **8**, 497–503 (2007).
26. Franchi, L. *et al.* Calcium-independent phospholipase A2β is dispensable in inflammasome activation and its inhibition by bromoenol lactone. *J. Innate Immun.* **1**, 607–617 (2009).
27. Qu, Y. *et al.* Phosphorylation of NLRC4 is critical for inflammasome activation. *Nature* **490**, 539–542 (2012).
28. Gross, O. *et al.* Syk kinase signalling couples to the Nlrp3 inflammasome for anti-fungal host defence. *Nature* **459**, 433–436 (2009).
29. Shio, M.T. *et al.* Malarial hemozoin activates the NLRP3 inflammasome through Lyn and Syk kinases. *PLoS Pathog.* **5**, e1000559 (2009).
30. Chuang, Y.T. *et al.* Tumor suppressor death-associated protein kinase is required for full IL-1β production. *Blood* **117**, 960–970 (2011).
31. Kankkunen, P. *et al.* (1,3)-beta-glucans activate both dectin-1 and NLRP3 inflammasome in human macrophages. *J. Immunol.* **184**, 6335–6342 (2010).
32. Lu, B. *et al.* Novel role of PKR in inflammasome activation and HMGB1 release. *Nature* **488**, 670–674 (2012).
33. Wong, K.W. & Jacobs, W.R. Jr. Critical role for NLRP3 in necrotic death triggered by *Mycobacterium tuberculosis*. *Cell Microbiol.* **13**, 1371–1384 (2011).
34. Stehlik, C. *et al.* The PAAD/PYRIN-only protein POP1/ASC2 is a modulator of ASC-mediated nuclear-factor-κB and pro-caspase-1 regulation. *Biochem. J.* **373**, 101–113 (2003).
35. Kosako, H. *et al.* Phosphoproteomics reveals new ERK MAP kinase targets and links ERK to nucleoporin-mediated nuclear transport. *Nat. Struct. Mol. Biol.* **16**, 1026–1035 (2009).
36. Kurokawa, M. & Kornbluth, S. Caspases and kinases in a death grip. *Cell* **138**, 838–854 (2009).
37. Sumbayev, V.V. & Yasinska, I.M. Role of MAP kinase-dependent apoptotic pathway in innate immune responses and viral infection. *Scand. J. Immunol.* **63**, 391–400 (2006).
38. Balci-Peynircioglu, B. *et al.* Expression of ASC in renal tissues of familial mediterranean fever patients with amyloidosis: postulating a role for ASC in AA type amyloid deposition. *Exp. Biol. Med. (Maywood)* **233**, 1324–1333 (2008).
39. Villani, A.C. *et al.* Common variants in the NLRP3 region contribute to Crohn's disease susceptibility. *Nat. Genet.* **41**, 71–76 (2009).
40. Zaki, M.H. *et al.* The NLRP3 inflammasome protects against loss of epithelial integrity and mortality during experimental colitis. *Immunity* **32**, 379–391 (2010).
41. Jin, Y. *et al.* NALP1 in vitiligo-associated multiple autoimmune disease. *N. Engl. J. Med.* **356**, 1216–1225 (2007).
42. Vandanmagsar, B. *et al.* The NLRP3 inflammasome instigates obesity-induced inflammation and insulin resistance. *Nat. Med.* **17**, 179–188 (2011).
43. Duewell, P. *et al.* NLRP3 inflammasomes are required for atherogenesis and activated by cholesterol crystals. *Nature* **464**, 1357–1361 (2010).
44. Pope, R.M. & Tschopp, J. The role of interleukin-1 and the inflammasome in gout: implications for therapy. *Arthritis Rheum.* **56**, 3183–3188 (2007).

ONLINE METHODS

Mice. Female wild-type, *Casp1*$^{-/-}$, *Pycard*$^{-/-}$, *Nlrp3*$^{-/-}$, *Card9*$^{-/-}$, *Mapk8*$^{-/-}$ and *Mapk9*$^{-/-}$C57BL/6J mice were maintained in specific pathogen–free conditions and were used at 6–9 weeks of age[12,16,45,46]. C57BL/6J mice heterozygous for the *Syk*^{tm1Tyb} allele[47] were intercrossed to generate embryos at embryonic day 16.5 that were wild-type for *Syk* (*Syk*$^{+/+}$) or heterozygous or homozygous for the *Syk*^{tm1Tyb} allele (*Syk*$^{+/-}$ or *Syk*$^{-/-}$). Fetal liver cells from those embryos were used to reconstitute C57BL/6J mice that had been irradiated with a total dose of 10 Gy from a ^{137}Cs source. Bone marrow cells from wild-type, *Mapk8*$^{-/-}$ or *Mapk9*$^{-/-}$ mice were also used to reconstitute irradiated C57BL/6J mice. Mice were used 6–7 weeks after reconstitution. All the experimental procedures performed on mice were approved by the Animal Ethics and Research Committee of Kyoto University Graduate School of Medicine.

Cells. Peritoneal macrophages, bone marrow–derived macrophages and bone marrow–derived dendritic cells were prepared as reported[48,49]. Those cells suspended in culture medium consisted of RPMI-1640 medium supplemented with 10% FCS and 10 μg/ml gentamicin were incubated on culture plates overnight at 37 °C, then were used for this study. U937 cells (provided by M. Matsuura) were cultured for 3 d in culture medium supplemented with 10 ng/ml of 12-*O*-tetradecanoylphorbol 13-acetate, 100 U/ml of penicillin and 100 μg/ml of streptomycin. The order of treatment and positions of wells in multiwell devices were determined randomly.

Reagents. LPS and flagellin were from Invivogen; alum was from Pierce; nigericin and poly(dA:dT) were from Sigma-Aldrich; MSU was from Nacalai Tesque; R406 was from Selleckchem; other kinase inhibitors were from Merck Biosciences; and BHA (butylated hydroxyanisole) was from Wako. Polyclonal antibody to ASC (AL177) and mouse monoclonal antibody (mAb) to NLRP3 (Cryo-2) were from Alexis; mAb to Jnk (56G8), mAb to phosphorylated Jnk (81E11) and mouse mAb to phosphorylated Jnk (G9) were from Cell Signaling Technology; mAb to phosphorylated Tyr (PY20), antibody to caspase-1 p10 (M-20) and antibody to Syk (anti-Syk) (N-19) were from Santa Cruz; anti-Flag (600-401-383) was from Rockland Immunochemicals; biotin-conjugated anti-IL-1β (BAF401) was from R&D Systems; and mAb to IL-18 (39-3F) was from MBL. The enzyme-linked immunosorbent assay kit for mouse IL-1β was from eBioscience. For the 'titration' of human or mouse IL-18, a pair of biotin-labeled (93-10C) and unlabeled (74) monoclonal antibodies to IL-18 was used (both from MBL).

Plasmids. The plasmid pmax-GFP was from Lonza. The pFLAG expression vectors for ASC, pro-caspase-1, and pro-IL-1β were constructed before[16]. The expression vectors for NLRP3 (R258W), Syk, Jnk1 (isoform β2) and Jnk2 (isoform β2) were constructed with primer sets (**Supplementary Table 3**) and the pFLAG-CMV2 vector (Sigma-Aldrich). After that construction, the mutation in the gene encoding NLRP3 or ASC was introduced into each expression vector by site-directed mutagenesis. Similarly, pFLAG–pro-caspase-1 and pFLAG–pro-IL-1β in which the Flag tag was removed were generated.

Stimulation with inflammasome activators. Cells were plated at a density of 5 × 10^5 cells per well in 24-well microplates. Culture medium was replaced with Opti-MEM (Invitrogen) before stimulation or infection. Macrophages were primed for 4 h with 50 ng/ml LPS and stimulated with nigericin (5 μM) or alum (500 μg/ml). For delivery into the cytosol of macrophages, flagellin (15 ng) was encapsulated into Sendai virus envelope with GenomONE-Neo (Ishihara Sangyo). Poly(dA:dT) (2.6 μg/ml) was introduced into unprimed macrophages through the use of Lipofectamine LTX (Invitrogen). Cells were infected with *L. monocytogenes* EGD[48] (multiplicity of infection, 1) or *S.* Typhimurium 14028 (multiplicity of infection, 10), and gentamicin was added to the cultures 30 min after infection. Cells infected with *M. tuberculosis* H37Rv (multiplicity of infection, 5) were washed 3 h after infection and were further cultivated in Opti-MEM containing gentamicin. Kinase inhibitors or dimethyl sulfoxide were added to cell cultures 1 h before stimulation or infection for inflammasome activation.

Immunoblot analysis. Cells were lysed with SDS sample buffer. Supernatants were concentrated with trichloroacetate. For the generation of Triton X-100–soluble and Triton X-100–insoluble fractions, cells were lysed with 50 mM Tris-HCl (pH 7.6) containing 0.5% Triton X-100, EDTA-free protease inhibitor 'cocktail' and phosphatase inhibitor 'cocktail' (Nacalai tesque). The lysates were centrifuged at 6,000*g* at 4 °C for 15 min, and the pellets and supernatants were used as the Triton-insoluble and Triton-soluble fractions, respectively. For the detection of phosphorylated Syk, total Syk was immunoprecipitated with anti-Syk (N-19; Santa Cruz) and protein G Sepharose (GE Healthcare).

Crosslinkage of ASC dimers or oligomers. The Triton-insoluble pellets were washed twice with Tris-buffered saline and then resuspended in 500 μl Tris-buffered saline. The resuspended pellets were crosslinked for 45 min at 37 °C with 2 mM disuccinimidyl suberate (Pierce) and then centrifuged for 15 min at 6,000*g*. The pellets were dissolved in SDS sample buffer.

Enrichment of phosphorylated proteins. Phosphorylated proteins were enriched from cell lysates with a Pro-Q Diamond Phosphoprotein Enrichment Kit according to the manufacturer's instructions (Invitrogen). Cells were lysed in lysis buffer supplemented with inhibitors of endonuclease and proteinase, then ASC aggregates were solubilized with 8 M urea. After centrifugation for 10 min at 10,000*g*, the supernatants were applied to the Pro-Q diamond column (1 mg protein per column). The column was washed and eluted with elution buffer (50 mM Tris, 2% SDS, 10 mM EDTA and 5% 2-mercaptoethanol, pH 8). The flow-through and elution fractions were concentrated with trichloroacetate. ASC or phosphorylated tyrosine in each fraction was detected by immunoblot analysis.

Phos-tag-based MSA. The Triton X-100–insoluble and Triton X-100–soluble fractions from macrophages (prepared as described above) were analyzed by Phos-tag MSA. HEK293 cells were lysed with 50 mM Tris-HCl (pH 7.6) containing 1% SDS, then lysates were precipitated with isopropanol and acetone. Proteins in the lysates were precipitated with acetone, incubated overnight at 37 °C in phosphatase reaction mixture containing 250 U/ml of antarctic phosphatase (New England BioLabs), reprecipitated with acetone and dissolved in SDS sample buffer. Those samples were separated by electrophoresis through 12% polyacrylamide gels with or without 50 μM $MnCl_2$ and 25 μM Phos-tag ligand (NARD Institute).

RNA-mediated interference. Cells were transfected with 30 nM small interfering RNA through the use of the siPORT Amine Transfection Agent (Ambion) as reported[16]. After 48 h of cultivation, the cells were washed and used in experiments. The sense small interfering RNA sequences were as follows: *Syk* (A), ACUUGUAGUAGUUGAUGCAUUCGGG; *Syk* (B), AUUCCGAUCAUGCG CACAAUGUAGG; *Mapk8* (A), AAUAUAGUCCCUUCCUGGAAAGAGG; *Mapk8* (B), AAUUCCAGCAGAGUGAAGGUGCUUG; *Mapk9* (A), UAAA GUUGGUACAGGCUGUUCGCGC; and *Mapk9* (B), UUCAAUCGCAUGC UCUCUUUCUUCC. Stealth RNAi negative control medium GC duplex #3 was from Invitrogen.

Immunofluorescence staining. Cells seeded in eight-well chamber plates at a density of 2.5 × 10^5 cells per well were washed twice, fixed in 4% paraformaldehyde and permeabilized with 0.25% Triton X-100. The cells were incubated with anti-ASC (AL177; Alexis) and then with Alexa 488-labeled or Alexa 594-labeled antibody to rabbit IgG (A11034 or A11012; Invitrogen). Nuclei were stained with DAPI (4,6-diamidino-2-phenylindole; Dojindo).

***In situ* PLA.** Fixed and permeabilized cells were incubated overnight at 4 °C with the following pairs of primary antibodies: rabbit anti-ASC (AL177; Alexis) together with mouse mAb to phosphorylated Jnk (G9; Cell Signaling) or mouse mAb to NLRP3 (Cryo-2; Alexis). The cells were washed and allowed to react to a pair of proximity probes (Olink Bioscience). The rest of the *in situ* PLA protocol was performed according to the manufacturer's instructions. The cells were examined by fluorescence microscopy (Olympus), and the Duolink Image Tool (Olink Bioscience) was used for quantitative analysis.

Reconstruction of the inflammasome system in HEK293 cells. HEK293 cells (CRL-1573; American Type Culture Collection) were maintained in DMEM supplemented with 10% FCS, 6 mM L-glutamine, 1 mM sodium pyruvate and

doi:10.1038/ni.2749

5 μg/ml gentamicin as described[16]. For experiments, HEK293 cells were plated in 24-well microplates at a density of 2×10^5 cells per well and incubated overnight. The cells were transfected with plasmids through the use of Transfectin according to the manufacturer's instructions (Bio-Rad). The total amount of DNA was adjusted to a concentration of 1 μg per well with pFLAG-CMV2 empty vector. The cells were washed with culture medium 36 h after transfection and were further incubated for 12 h.

Reconstruction in macrophages. RAW264.7 cells (provided by H. Tanizaki) or primary *Pycard*$^{-/-}$ peritoneal macrophages were transfected with 1,000 ng of pFLAG-ASC or the ASC mutant vectors together with pFLAG-NLRP3 (R258W) (250 ng) through the use of the Neon Transfection System according to the manufacturer's instructions (Invitrogen). Electroporation parameters were as follows: pulse voltage, 1,680 V; pulse width, 20 ms; pulse number, 1; cell number, 1×10^6. The cells were incubated for 9 h.

Peritonitis. Mice were challenged intraperitoneally with MSU (1 mg) or alum (0.4 mg). At 2 h before and 30 min after challenge with the irritants, wild-type mice were treated intraperitoneally with dimethyl sulfoxide or the Jnk inhibitor SP600125 (25 mg per kg body weight). The mice were killed 6 h after injection of the stimuli, and peritoneal cavities were lavaged with 5 ml PBS. Mice were given intraperitoneal injection of mouse CXCL1 (0.8 μg; BioLegend) or PBS, and peritoneal cells were collected 1.5 h after stimulation. Peritoneal cells were counted with a Countess (Invitrogen) and then were allowed to react to mAb to mouse CD16 (93; BioLegend). The cells were subsequently stained with fluorescein isothiocyanate–labeled mAb to Gr-1 (RB6-8C5; BioLegend) and phycoerythrin-labeled mAb to F4/80 (BM8; BioLegend) and were analyzed on a FACSCalibur (Becton Dickinson). Mice were prepared by H.H. and were randomly assigned to experimental groups. Another investigator (R.F.), who did the injections and flow cytometry, was 'blinded' to the identity of the groups.

Statistical analysis. The sample size of *in vivo* and *in vitro* studies was chosen to be as small as possible but to allow the evaluation of distribution normality. For two-group comparisons by Gaussian distribution, a two-tailed unpaired *t*-test with Welch's correction was used when the variances of the groups were judged to be equal by the *F* test. For two-group comparisons with non-Gaussian distribution, a Mann-Whitney test was used. Multigroup comparisons with Gaussian distribution, one-way ANOVA with Bonferroni's multiple-comparison test or Tukey-Kramer's multiple-comparison test (for samples of unequal size) was used after the confirmation of homogeneity of variance among the groups by Bartlett's test. For multigroup comparisons with non-Gaussian distribution, a Kruskal-Wallis test with Dunn's test was used. *P* values of 0.05 or less were the threshold for statistical significance.

45. Hara, H. *et al.* The adaptor protein CARD9 is essential for the activation of myeloid cells through ITAM-associated and Toll-like receptors. *Nat. Immunol.* **8**, 619–629 (2007).
46. Cao, Y. *et al.* Enhanced T cell-independent antibody responses in c-Jun N-terminal kinase 2 (JNK2)-deficient B cells following stimulation with CpG-1826 and anti-IgM. *Immunol. Lett.* **132**, 38–44 (2010).
47. Turner, M. *et al.* Perinatal lethality and blocked B-cell development in mice lacking the tyrosine kinase Syk. *Nature* **378**, 298–302 (1995).
48. Hara, H. *et al.* Dependency of caspase-1 activation induced in macrophages by *Listeria monocytogenes* on cytolysin, listeriolysin O, after evasion from phagosome into the cytoplasm. *J. Immunol.* **180**, 7859–7868 (2008).
49. Lutz, M.B. *et al.* An advanced culture method for generating large quantities of highly pure dendritic cells from mouse bone marrow. *J. Immunol. Methods* **223**, 77–92 (1999).

PLOS | NEGLECTED TROPICAL DISEASES

Characterization of a Gene Family Encoding SEA (Sea-urchin Sperm Protein, Enterokinase and Agrin)-Domain Proteins with Lectin-Like and Heme-Binding Properties from *Schistosoma japonicum*

Evaristus Chibunna Mbanefo[1,2], Mihoko Kikuchi[1], Nguyen Tien Huy[1], Mohammed Nasir Shuaibu[1], Mahamoud Sama Cherif[1], Chuanxin Yu[3], Masahiro Wakao[4], Yasuo Suda[4,5], Kenji Hirayama[1]*

1 Department of Immunogenetics, Institute of Tropical Medicine (NEKKEN) and Global COE Program, Nagasaki University, Sakamoto, Japan, **2** Department of Parasitology and Entomology, Faculty of Bioscience, Nnamdi Azikiwe University, Awka, Nigeria, **3** Laboratory on Technology for Parasitic Disease Prevention and Control, Jiangsu Institute of Parasitic Diseases, Meiyuan, Wuxi, People's Republic of China, **4** Department of Chemistry, Biotechnology and Chemical Engineering, Graduate School of Science and Engineering, Kagoshima University, Kohrimoto, Kagoshima, Japan, **5** SUDx-Biotec Corporation, Shiroyama, Kagoshima, Japan

Abstract

Background: We previously identified a novel gene family dispersed in the genome of *Schistosoma japonicum* by retrotransposon-mediated gene duplication mechanism. Although many transcripts were identified, no homolog was readily identifiable from sequence information.

Methodology/Principal Findings: Here, we utilized structural homology modeling and biochemical methods to identify remote homologs, and characterized the gene products as SEA (sea-urchin sperm protein, enterokinase and agrin)-domain containing proteins. A common extracellular domain in this family was structurally similar to SEA-domain. SEA-domain is primarily a structural domain, known to assist or regulate binding to glycans. Recombinant proteins from three members of this gene family specifically interacted with glycosaminoglycans with high affinity, with potential implication in ligand acquisition and immune evasion. Similar approach was used to identify a heme-binding site on the SEA-domain. The heme-binding mode showed heme molecule inserted into a hydrophobic pocket, with heme iron putatively coordinated to two histidine axial ligands. Heme-binding properties were confirmed using biochemical assays and UV-visible absorption spectroscopy, which showed high affinity heme-binding ($K_D = 1.605 \times 10^{-6}$ M) and cognate spectroscopic attributes of hexa-coordinated heme iron. The native proteins were oligomers, antigenic, and are localized on adult worm teguments and gastrodermis; major host-parasite interfaces and site for heme detoxification and acquisition.

Conclusions: The results suggest potential role, at least in the nucleation step of heme crystallization (hemozoin formation), and as receptors for heme uptake. Survival strategies exploited by parasites, including heme homeostasis mechanism in hemoparasites, are paramount for successful parasitism. Thus, assessing prospects for application in disease intervention is warranted.

Citation: Mbanefo EC, Kikuchi M, Huy NT, Shuaibu MN, Cherif MS, et al. (2014) Characterization of a Gene Family Encoding SEA (Sea-urchin Sperm Protein, Enterokinase and Agrin)-Domain Proteins with Lectin-Like and Heme-Binding Properties from *Schistosoma japonicum*. PLoS Negl Trop Dis 8(1): e2644. doi:10.1371/journal.pntd.0002644

Editor: Aaron R. Jex, University of Melbourne, Australia

Received August 24, 2013; **Accepted** November 28, 2013; **Published** January 9, 2014

Funding: ECM is a recipient of the Japanese Government Ministry of Education, Culture, Science and Technology (MEXT) PhD fellowship. This study was supported in part by the GCOE Program (2008–2011) and Grant-in-Aid for 21st century COE program (2003–2008), Nagasaki University; and Grant-in-Aid for Scientific Research B (22406009) and C (23590489) from Japanese Government Ministry of Education, Culture, Science and Technology (MEXT). The funders had no role in study design, data collection and analysis, decision to publish, or preparation of the manuscript.

Competing Interests: The authors have declared that no competing interests exist.

* E-mail: hiraken@nagasaki-u.ac.jp

Introduction

Schistosomiasis still ranks as the most important helminthic infection; second only to malaria in its socioeconomic burden in the resource constrained tropics and subtropics. It affects over 200 million people worldwide with more than 700 million people at risk of getting infected [1]. Although an effective treatment is available (praziquantel), the fact that reinfection occurs very rapidly after mass treatment renders chemotherapy alone inadequate for disease control. It is opined that a prophylactic alternative applied singly or in combination with other interventions, even with limited efficacy in limiting transmission is the optimum approach [2]. This intervention is especially needed in *S. japonicum* endemic areas, where non-human mammalian hosts are complicating control efforts.

Schistosomes inhabit host vasculature, where they ingest erythrocytes and catabolize the host hemoglobin as a source of amino acids for their growth, development and reproduction [3]. However, large quantities of potentially toxic heme (Fe-protoporphyrin IX) are released as 'byproducts' of hemoglobinolysis [3–6].

Author Summary

While isolating membrane-bound and secreted proteins as targets for *Schistosoma japonicum* vaccine, we identified a novel potentially functional gene family which had originated by a gene duplication mechanism. Here, we integrated structural homology modeling and biochemical methods to show that this gene family encodes proteins with sea-urchin sperm protein, enterokinase and agrin (SEA) –domain, with heme-binding properties. Typical of SEA-structural domains, the characterized proteins specifically interacted with glycosaminoglycans (GAGs), with implication in ligand gathering and immune-evasion. Consistent with modeled heme-binding pocket, we observed high affinity heme-binding and spectroscopic attributes of hexa-coordinated heme iron. Localization of the native gene-products on adult worm tegument and gastrodermis, host interfaces for heme-sequestration and acquisition, suggests potential roles for this gene family in heme-detoxification and heme-iron uptake.

The parasite is thus faced with the challenge of maintaining heme homeostasis by evolving strategies to sequester and detoxify heme [3,5–9], and at the same time maintaining a heme acquisition mechanism to harness the needed iron from the heme molecules [4,10]. Indeed, effective mechanisms for detoxification of toxic heme and controlled acquisition of heme iron are paramount for parasite survival and establishment. Such mechanisms are major targets of effective drugs against hemoparasites, including malaria and schistosomiasis [11–13]. However, information on the exact mechanisms and molecules involved in this 'weak link' is either lacking or equivocal [3]. Such molecular targets should be localized at the host-parasite interfaces in contact with the host erythrocytes.

The tegument and gastrodermis are syncytial layers lining the entire parasite surface and the parasite gut, respectively [14–16]. Heme liberated during hemoglobinolysis is sequestered in the parasite gastrodermis lining the gut lumen [4,17], and subsequently detoxified to non-toxic crystalline aggregates called hemozoin [8,9,17,18] and regurgitated. The exact mechanism is not fully understood but it is thought that heme-binding proteins initiate the nucleation step of the crystallization, while lipids mediate the elongation step in an amphiphilic interface created by lipid droplets in the gastrodermis and gut lumen [17,19]. Equally, schistosomes like other obligate parasites scavenge molecules from the host, including heme as the major source of iron needed for development and reproduction [4,10]. Also, newly penetrated schistosomulae obtain iron via heme-binding proteins on their teguments before their guts are developed [20]. Thus, heme-binding proteins that are localized at these interfaces are most likely involved in the parasite heme acquisition and detoxification.

Over the years, enormous resources and technologies have been channeled towards identifying molecular targets involved in several biological mechanisms utilized by parasites for effective parasitism. The recently completed genome [21], transcriptome sequences [22] and proteomic studies [23] of this parasite represent invaluable feats towards identifying such targets. Although the functions of many sequenced genes are readily known or inferred from their amino acid sequences, many of the genes that are potential determinants of successful parasitism sometimes do not have readily identifiable sequence homologs. This is a major challenge for placing the vast amount of *'omics'* data into functional contexts for identifying genes of interest [24,25]. As a matter of fact, several of such proteins presently annotated as 'hypothetical proteins' may well represent the missing link to filling the gene 'gaps' in our understanding of host-parasite interactions. Indeed, over 30% of *S. japonicum* proteins are yet of unknown functions [21]. Therefore, adopting novel strategies for the characterization of otherwise 'hypothetical proteins' is highly needed and can provide valuable functional clues that may not be readily identifiable from sequence data alone [24,25].

Our group had utilized a signal sequence trap (SST) to isolate secreted and membrane binding antigens from *S. japonicum* with appreciable success [26]. Among the SST isolated candidates, we identified a novel gene family which we found to have originated through a repetitive element mediated DNA-level gene duplication mechanism [27]. Although several transcripts from ~27 duplicons were identified, no sequence homolog was readily identifiable in other organisms. We here utilized an integrated strategy combining comparative structural homology modeling and biochemical analyses to identify remote structural homologs, and characterize an extracellular domain in this family as SEA (**s**ea urchin sperm protein, **e**nterokinase and **a**grin)-domain. Similar approach was used to further identify and characterize a functional heme-binding site on the SEA-domain. SEA-module is an extracellular structural domain originally identified in **s**ea urchin **s**perm protein, **e**nterokinase and **a**grin, the basis for the nomenclature [28–30]. The domain is found in several functionally diverse proteins, and is known to assist or regulate binding to carbohydrate moieties. SEA-domain evolved from the ancestral ferredoxin-like fold, which is able to acquire various active sites including heme-binding sites [24]. The identification of a functional heme-binding protein in this hemophagous trematode is a significant contribution to our understanding of the host-parasite interaction as regards heme homeostasis. The biological significance of this finding and the potential role of this gene family in parasitism are discussed in terms of the parasite biology and prospects for application in disease intervention.

Materials and Methods

Ethics statement

This study adhered strictly to the recommendations in the Fundamental Guidelines for Proper Conduct of Animal Experiment and Related Activities in Academic Research Institutions under the jurisdiction of the Ministry of Education, Culture, Sports, Science and Technology, Japan (Notice No: 71). All animal experiments were approved by Nagasaki University Board of Animal Research, according to Japanese guidelines for use of experimental animals (Approval No: 0809050699).

Experimental animals

Six to eight weeks old Female BALB/c mice were purchased from SLC Inc. Labs, Japan. The CLAWN strain miniature pigs were from Japan Farm, Kagoshima, Japan. The miniature pigs were infected percutaneously with 200 *S. japonicum* cercariae.

Molecular structure modeling and ligand-binding characterization

Multiple alignments were performed using NCBI BLAST and *Multialin* Interface [31]. Post translational modifications were predicted using YingOYang 1.2 [32]. Molecular structure modeling was performed by fold recognition and *ab-initio* structure prediction methods using Protein Homology/Analogy Recognition Engine (*Phyre* v2.0) [33] and *Rosetta* Full Chain Protein Structure Prediction Server [34]. Ligand binding analysis to identify potential ligands and their binding sites in the folded protein was performed using *3DLigandSite* server [35]. The

modeled structures were analyzed using Discovery Suite 3.5 Molecular Visualizer, while the modeled receptor-ligand interactions were analyzed on the PyMol Molecular Graphics System, Version 1.6 (Schrodinger, LLC).

Total RNA isolation, cDNA synthesis and quantitative real-time PCR

Total mRNA was purified from parasite egg, sporocyst, cercaria and schistosomula using Micro-to-Midi total RNA purification system (Invitrogen, USA), and from adult worms using NucleoSpin RNA II kit (Macherey-Nagel, Germany). Reverse transcription and amplification of the double stranded cDNAs were performed using Ovation Pico WTA System v2 (NuGEN, USA). For each candidate gene and the reference gene (*S. japonicum* β-Actin), PCR fragment was first cloned into pCR2.1 cloning vector and the resulting constructs used as templates for qPCR standards and for estimation of copy numbers. Relative expression of candidate genes in different developmental stages of the parasite was quantified using SYBR Premix *Ex Taq* II Reagents (Takara, Japan). Real-time PCR and data analysis were performed on AB 7500 Real-Time PCR Systems v2.0.5.

Cloning, expression and purification of recombinant protein

The complete coding sequences of the candidates were amplified and cloned into the TOPO TA cloning site of the expression vector pcDNA4/HisMax and expressed in BL21 *E. coli* cells, and FreeStyle 293 expression system (Invitrogen, USA) for binding assays. We took advantage of His6 tag to purify the recombinant proteins using TALON Metal Affinity Resins (Clontech, USA). Purified proteins were concentrated and imidazole elution buffer exchanged using Amicon Ultra Centrifugal Filters (Millipore, USA). Size exclusion gel filtration was performed using Sephadex G-50 medium (GE healthcare, USA). For heme-binding assays, purified proteins from FreeStyle 293 cells were treated with enterokinase to remove tags and purified with EK-Away resin (Invitrogen, USA).

Preparation of specific immune serum and monoclonal antibodies

Polyclonal mouse sera were produced against recombinant antigens by subcutaneous immunization of mice with 25 μg of purified recombinant proteins in 50 μl PBS, mixed with an equal volume of Gerbu Adjuvant 100 (GERBU Biotechnik, Denmark), on days 0, 21 and 42. Two weeks after the last inoculation, mice were exsanguinated to collect sera and spleens were aseptically obtained for monoclonal antibody preparation using the Clonacell-HY system (Stemcell Technologies, USA), according to manufacturer's instructions. The monoclonal antibodies were biotinylated using the one-step antibody biotinylation kit (Mitenylbiotech, USA).

Immunolocalization

Freshly perfused adult *S. japonicum* were washed three times in PBS (pH 7.4) and fixed in 4% neutral paraformaldehyde at 4°C until use. The samples were alcohol dehydrated, embedded in paraffin, cut into 5–7 μm thin sections and then mounted on microscope glass slides. Paraffin sections were deparaffinized by incubating for 10 min in two changes of xylene and rehydrated by sequential 10 min incubations in 100%, 95%, 70% and 50% ethanol, before rinsing in two changes of double deionized water. Schistosomulae were prepared by mechanical transformation and washed in Hanks solution. After washing with distilled water, the juvenile worms were fixed in cold acetone for 2 hours. Two drops of acetone fixed schistosomulae were added to poly-L-lysine coated glass slides and dried overnight. Immunoperoxidase technique was then performed as in adult worm sections.

Immunoperoxidase staining and immunofluorescence assays were performed using minor modifications to the method detailed by [36]. Briefly, the sections for immunoperoxidase staining were treated with 3% H_2O_2 in PBS for 30 min to destroy endogenous peroxidase. All sections were blocked for non-specific binding with 5% skim milk in PBS for 1 h, and then incubated for 2 h at room temperature with biotinylated monoclonal antibody or immune sera as indicated in each case. After washing three times in PBS pH 7.4 for 5 min each, the sections were incubated in FITC conjugated secondary antibody for immune sera IFA. For biotinylated mAB IFA and immunoperoxidase assays, sections were incubated for 30 mins with streptavidin-FITC (1:500) and streptavidin-HRP (1:500) solution respectively. The immunoperoxidase sections were washed in PBS and treated with diaminobenzidine tetrahydrochloride (DAB) chromogen, according to manufacturer's instructions (Dako, Japan). After counterstaining immunoperoxidase sections with Mayer hematoxylin, all the sections were washed, dehydrated by passage through alcohol and xylene, mounted, and viewed under Keyence All-in-one Fluorescence Microscope (Keyence, USA). Pre-immune serum was used as negative control.

Glycoprotein detection

For glycoprotein detection assay, SDS-PAGE fractionated purified recombinant proteins were stained using the Pierce Glycoprotein Staining Kit (Thermo Scientific, USA).

Glycan binding analysis using Surface Plasmon Resonance (SPR)

We utilized array type sugar chip (SUDx-Biotec, Japan); which is an array of 48 structurally defined sugar chains (glycans) immobilized on a thin gold chip to analyze the interactions of the SEA-domain proteins with glycans using SPR imaging [37]. The surface plasmon is excited when light is focused on the opposite side of the chip. The reflective light is measurable and is altered in response to binding of the proteins to the immobilized glycans. This alteration of the surface plasmon (expressed as resonance units, RU) is directly proportional to change in bound mass of analytes. Real time measuring of the SPR RU was used to monitor changes in the surface concentration or amount of bound analytes (protein). One of the benefits of this SPR system is that the weak interactions, which are easily washed out in the regular array technology and therefore not recognized, can also be monitored in real time. We used this method to detect real-time biological interactions between several glycans and the characterized SEA-domain proteins. For assessing the specificity and affinity of the protein-glycan interactions, we used chondroitin sulfate GAG chip to measure the association and dissociation kinetics in real time to determine K_D of the binding.

Hemin-agarose binding assay

Hemin-agarose binding assay was applied to study heme binding as detailed by [38]. Briefly, 200 μl of hemin-agarose (Sigma-Aldrich, USA) was washed three times in 1 ml of 100 mM NaCl-25 mM Tris-HCl (pH 7.4) with centrifugation done at 750×*g* for 5 min. Hemin-agarose was incubated with protein (20 μg) for 1 h at 37°C with gentle mixing. After 4 washes to remove unbound proteins, the beads were incubated for 2 min with elution solution (2% (wt/vol) SDS and 1% (vol/vol)